Likely oscillatory motions of stochastic hyperelastic spherical shells and tubes

L. Angela Mihai* Manal Alamoudi†

January 4, 2021

Abstract

We examine theoretically the dynamic inflation and finite amplitude oscillatory motion of inhomogeneous spherical shells and cylindrical tubes of stochastic hyperelastic material. These bodies are deformed by radially symmetric uniform inflation, and are subjected to either a surface dead load or an impulse traction, uniformly applied in the radial direction. We consider composite shells and tubes with two concentric stochastic homogeneous neo-Hookean phases, and inhomogeneous bodies of stochastic neo-Hookean material with constitutive parameters varying continuously in the radial direction. For the homogeneous materials, we define the elastic parameters as spatially-independent random variables, while for the radially inhomogeneous bodies, we take the parameters as spatially-dependent random fields, described by non-Gaussian probability density functions. Under radially symmetric dynamic deformation treated as quasi-equilibrated motion, we show that the bodies oscillate, i.e., the radius increases up to a point, then decreases, then increases again, and so on, and the amplitude and period of the oscillations are characterised by probability distributions, depending on the initial conditions, the geometry, and the probabilistic material properties.

Key words: stochastic elasticity, finite strain analysis, quasi-equilibrated motion, probabilities.

1 Introduction

The extensive study of oscillatory motions of cylindrical or spherical shells of linear elastic material has been driven by a wide range of industrial applications [3, 4, 10, 14]. In contrast, time-dependent finite oscillations of cylindrical tubes and spherical shells of nonlinear elastic material have received less attention. Internally pressurised hollow cylinders and spheres are relevant in many biological and engineering structures [21,76]. Cylindrical tubes of homogeneous isotropic incompressible hyperelastic material subject to finite symmetric inflation and stretching were first analysed in [56]. For elastic spherical shells, finite radially symmetric inflation was investigated initially in [23], then in [2, 60]. For both elastic tubes and spherical shells, in [12], it was shown that, depending on the particular material and initial geometry, the internal pressure may increase monotonically, or increase and then decrease, or increase, decrease, and then increase again. Further studies examining these deformations for different constitutive descriptions can be found in [22, 51, 79]. Localised bulging in long inflated isotropic hyperelastic tubes of arbitrary thickness was modelled and analysed within the framework of nonlinear elasticity in [19, 78].

The governing equations for large amplitude oscillations of spherical shells and tubes of homogeneous isotropic incompressible nonlinear hyperelastic material, formulated as special cases of *quasi-equilibrated motions* [74], were reviewed in [75]. These are the class of motions for which the deformation is circulation preserving, and at every time instant, the deformed configuration is a possible static configuration under the given forces. Free and forced axially symmetric radial oscillations of infinitely

*Corresponding author, School of Mathematics, Cardiff University, Senghennydd Road, Cardiff, CF24 4AG, UK, Email: MihaiLA@cardiff.ac.uk

†School of Mathematics, Cardiff University, Senghennydd Road, Cardiff, CF24 4AG, UK, Email: AlamoudiMO1@cardiff.ac.uk; College of Science and Humanities-Jubail, Imam Abdulrahman Bin Faisal University, Saudi Arabia, Email: malamoudi@iau.edu.sa

long, isotropic incompressible cylindrical tubes, with arbitrary wall thickness, were described for the first time in [34, 35]. For spherical shells, oscillatory motions were derived analogously in [26, 36, 77].

However, deterministic approaches, which are based on average data values, can greatly underestimate or overestimate mechanical responses, and stochastic representations accounting also for data dispersion are needed to improve assessment and predictions [20, 28, 33, 53, 55, 66, 73].

Recently, radial oscillations of cylindrical and spherical shells of hyperelastic material, treated as quasi-equilibrated motions, were reviewed and extended to stochastic hyperelastic bodies in [42, 49]. Namely, spherical and cylindrical shells of stochastic isotropic incompressible hyperelastic material were analysed in [42] where particular attention was given to the periodic (oscillatory) motion and time-dependent stresses taking into account the probabilistic model parameters. In [49], the cavitation and finite amplitude oscillations under radially symmetric finite deformation of homogeneous and radially inhomogeneous spheres of stochastic hyperelastic material was studied analytically.

Stochastic hyperelastic models are described by strain-energy densities with the parameters characterised by probability density functions (see [25, 68–72] and also [18, 46]). These are advanced phenomenological models that rely on the finite elasticity theory and on the notion of entropy [29–31,59,67] to enable the propagation of uncertainties from input data to output quantities of interest [65]. They can be also combined with Bayesian approaches [7, 40] for model selection [18, 46, 53, 57].

For stochastic homogeneous incompressible hyperelastic bodies, the effect of probabilistic model parameters on predicted mechanical responses was demonstrated theoretically on the various instability problems: the static cavitation of a sphere under uniform tensile dead load [43], the inflation of pressurised spherical and cylindrical shells [41], the classic problem of the Rivlin cube [47], the rotation and perversion of stochastic incompressible anisotropic hyperelastic cylindrical tubes [48]. In [43], in addition to the well-known case of stable cavitation post-bifurcation at the critical dead load, it was shown, for the first time, the existence of unstable (snap) cavitation for some (deterministic or stochastic) isotropic incompressible materials satisfying Baker-Ericksen inequalities [5]. In general, these problems, for which the elastic solutions are obtained explicitly, can offer significant insight into how the uncertainties in input parameters are propagated to output quantities. A similar stochastic methodology was developed to study instabilities in liquid crystal elastomers in [45]. To investigate the effect of probabilistic parameters in the case of more complex geometries and loading conditions, numerical approaches have been proposed in [71, 72].

For detailed presentations of the theory of nonlinear elasticity, we refer to [54,75]. A comprehensive review on nonlinear elastic material parameters in isotropic finite elasticity is provided in [44]. For probability theory, we rely on [24]. Relevant monographs on uncertainty quantification in solids are [15, 16, 66].

The scope of this study is to extend the analysis of [42,49] to large strain deformations and oscillatory motions of radially inhomogeneous cylindrical tubes and spherical shells of stochastic hyperelastic material. These bodies are deformed by radially symmetric uniform inflation when subject to either a surface dead load (which is constant in the reference configuration) or an impulse traction (which is maintained constant in the current configuration), applied uniformly in the radial direction. Section 2 provides a summary of the stochastic elasticity prerequisites, and introduces the notion of quasi-equilibrated motion. Section 3 is devoted to the analysis of finite amplitude oscillations of a composite formed from two concentric homogeneous tubes of different stochastic neo-Hookean material, and of inhomogeneous tubes with radially varying material properties. For spherical shells, a similar analysis is performed in Section 4. Numerical computations were carried out in Matlab, where inbuilt functions for random number generation were used. Concluding remarks are drawn in the final section.

2 Prerequisites

We first recall the definition of stochastic isotropic incompressible hyperelastic models and the notion of quasi-equilibrated motion.

2.1 Stochastic strain-energy functions for isotropic incompressible hyperelastic materials

For our general definition of stochastic isotropic incompressible hyperelastic materials, we rely on the following assumptions [18, 41–43, 46, 47, 49]:

(A1) Material objectivity, which requires that the constitutive equations must be invariant under changes of frame of reference. This means that the scalar strain-energy function, $W = W(\mathbf{F})$, depending only on the deformation gradient $\mathbf{F}$, with respect to the reference configuration, is unaffected by a superimposed rigid-body transformation after deformation. Material objectivity is guaranteed by defining strain-energy functions in terms of the scalar invariants.

(A2) Material isotropy, stating that the strain-energy function is unaffected by a superimposed rigid-body transformation prior to deformation. For isotropic materials, the strain-energy function is a symmetric function of the principal stretches.

(A3) Baker-Ericksen (BE) inequalities [5, 37], by which the greater principal Cauchy stress occurs in the direction of the greater principal stretch.

(A4) For any given finite deformation, at any point in the material, the shear modulus, μ, and its inverse, $1/\mu$, are second-order random variables, i.e., they have finite mean value and finite variance [68–72].

Assumptions (A1)-(A3) are inherited from the finite elasticity theory [21, 44, 54, 75], while (A4) places random variables at the foundation of stochastic hyperelastic models [46, 68–70]. A random variable is usually described in terms of its *mean value* and its *variance*, which contains information about the range of values about the mean value [11, 13, 28, 39, 52].

In order to derive analytical results for the instability problems presented here, we confine our attention to a class of stochastic hyperelastic models defined by the strain-energy density

$$\mathcal{W}(\lambda_1, \lambda_2, \lambda_3) = \frac{\mu}{2}\left(\lambda_1^2 + \lambda_2^2 + \lambda_3^2 - 3\right), \tag{1}$$

where the shear modulus, $\mu = \mu(R) > 0$, is a random field depending on the radius R in a system of cylindrical or spherical polar coordinates, and λ_1, λ_2, and λ_3 are the principal stretch ratios. When μ is independent of R, the material model (1) reduces to the stochastic (homogeneous) neo-Hookean model [46, 68].

For the shear modulus, $\mu = \mu(R)$, at any fixed R, we rely on the following available information, which guarantees that assumption (A4) holds [62–64, 66],

$$\begin{cases} E\left[\mu\right] = \underline{\mu} > 0, \\ E\left[\log\ \mu\right] = \nu, \quad \text{such that } |\nu| < +\infty. \end{cases} \tag{2}$$

By the principle of maximum entropy [29–31], for any fixed R, μ follows a Gamma probability distribution with the shape and scale parameters $\rho_1 = \rho_1(R) > 0$ and $\rho_2 = \rho_2(R) > 0$, respectively. Hence,

$$\underline{\mu} = \rho_1\rho_2, \qquad \mathrm{Var}[\mu] = \rho_1\rho_2^2, \tag{3}$$

where $\underline{\mu}$ is the mean value, $\mathrm{Var}[\mu] = \|\mu\|^2$ is the variance, and $\|\mu\|$ is the standard deviation of μ. The corresponding probability density function takes the form [1, 24, 32]

$$g(\mu; \rho_1, \rho_2) = \frac{\mu^{\rho_1 - 1} e^{-\mu/\rho_2}}{\rho_2^{\rho_1}\Gamma(\rho_1)}, \qquad \text{for } \mu > 0 \text{ and } \rho_1, \rho_2 > 0, \tag{4}$$

where $\Gamma : \mathbb{R}_+^* \to \mathbb{R}$ is the complete Gamma function

$$\Gamma(z) = \int_0^{+\infty} t^{z-1} e^{-t} \mathrm{d}t. \tag{5}$$

For ρ_1 and ρ_2, the word 'hyperparameters' is also used to distinguish them from the material parameter μ and other material constants [66, p. 8].

The stochastic shear modulus $\mu(R)$ will be illustrated in Sections 3.3 and 4.3 (see examples given by equations (57) and (108), respectively).

2.2 Quasi-equilibrated motion

For large strain dynamic deformations of an elastic solid, Cauchy's laws of motion are governed by the following Eulerian field equations [75, p. 40],

$$\rho\ddot{\mathbf{x}} = \text{div } \mathbf{T} + \rho\mathbf{b}, \tag{6}$$

$$\mathbf{T} = \mathbf{T}^T, \tag{7}$$

where ρ is the material density, which is assumed constant, $\mathbf{x} = \chi(\mathbf{X}, t)$ is the motion of the elastic solid, with velocity $\dot{\mathbf{x}} = \partial\chi(\mathbf{X}, t)/\partial t$ and acceleration $\ddot{\mathbf{x}} = \partial^2\chi(\mathbf{X}, t)/\partial t^2$, $\mathbf{b} = \mathbf{b}(\mathbf{x}, t)$ is the body force, $\mathbf{T} = \mathbf{T}(\mathbf{x}, t)$ is the Cauchy stress tensor, and the superscript 'T' is the transpose operator.

Definition 2.1 *[75, p. 208] A quasi-equilibrated motion, $\boldsymbol{x} = \chi(\boldsymbol{X}, t)$, is the motion of an incompressible homogeneous elastic solid subject to a given body force, $\boldsymbol{b} = \boldsymbol{b}(\boldsymbol{x}, t)$, whereby, for each value of t, $\boldsymbol{x} = \chi(\boldsymbol{X}, t)$ defines a static deformation that satisfies the equilibrium conditions under the body force $\boldsymbol{b} = \boldsymbol{b}(\boldsymbol{x}, t)$.*

Theorem 2.2 *[75, p. 208] (see also the proof in [42]) A quasi-equilibrated motion, $\boldsymbol{x} = \chi(\boldsymbol{X}, t)$, of an incompressible homogeneous elastic solid subject to a given body force, $\boldsymbol{b} = \boldsymbol{b}(\boldsymbol{x}, t)$, is dynamically possible, subject to the same body force, if and only if the motion is circulation preserving with a single-valued acceleration potential ξ, i.e.,*

$$\ddot{\boldsymbol{x}} = -\text{grad } \xi. \tag{8}$$

For the condition (8) *to be satisfied, it is necessary that*

$$\text{curl } \ddot{\boldsymbol{x}} = \boldsymbol{0}. \tag{9}$$

Then, the Cauchy stress tensor takes the form

$$\boldsymbol{T} = -\rho\xi\boldsymbol{I} + \boldsymbol{T}^{(0)}, \tag{10}$$

where $\boldsymbol{T}^{(0)}$ is the Cauchy stress for the equilibrium state at time t and $\boldsymbol{I} = diag(1, 1, 1)$ is the identity tensor. In this case, the stress field is determined by the present configuration alone. In particular, the shear stresses in the motion are the same as those of the equilibrium state at time t.

3 Quasi-equilibrated motion of stochastic cylindrical tubes

We examine here the quasi-equilibrated radial motion of two concentric homogeneous tubes and of a radially inhomogeneous tube with stochastic material parameters.

3.1 Radial-axial motion of a cylindrical tube

For a circular cylindrical tube, the combined radial and axial motion is described by

$$r^2 = c^2 + \frac{R^2 - C^2}{\alpha}, \qquad \theta = \Theta, \qquad z = \alpha Z, \tag{11}$$

where (R, Θ, Z) and (r, θ, z) are the cylindrical polar coordinates in the reference and current configuration, respectively, such that $C \leq R \leq B$, C and B are the inner and outer radii in the undeformed state, respectively, $c = c(t)$ and $b = b(t) = \sqrt{c^2 + (B^2 - C^2)/\alpha}$ are the inner and outer radius at time t, respectively, and $\alpha > 0$ is a given constant. When $\alpha = 1$, the time-dependent deformation (11) simplifies to that studied in [8, 34, 35]. The case with a time-dependent α was considered in [58].

The radial-axial motion (11) of a cylindrical tube is fully determined by the inner radius c at time t, which in turn is derived from the initial conditions. Thus, the acceleration $\ddot{r}$ can be obtained in

terms of the acceleration $\ddot{c}$ on the inner surface. By the governing equations (11), condition (9) is valid for $\mathbf{x} = (r, \theta, z)^T$. Hence, (11) describes a quasi-equilibrated motion, such that

$$-\frac{\partial \xi}{\partial r} = \ddot{r} = \frac{\dot{c}^2}{r} + \frac{c\ddot{c}}{r} - \frac{c^2\dot{c}^2}{r^3}, \tag{12}$$

where ξ is the acceleration potential satisfying (8). Integrating (12) gives [75, p. 215]

$$-\xi = \dot{c}^2 \log r + c\ddot{c} \log r + \frac{c^2\dot{c}^2}{2r^2} = \dot{r}^2 \log r + r\ddot{r} \log r + \frac{1}{2}\dot{r}^2. \tag{13}$$

The deformation gradient of (11), with respect to the polar coordinates (R, Θ, Z), is equal to

$$\mathbf{F} = \operatorname{diag}\left(\frac{R}{\alpha r}, \frac{r}{R}, \alpha\right), \tag{14}$$

the Cauchy-Green deformation tensor is

$$\mathbf{B} = \mathbf{F}^2 = \operatorname{diag}\left(\frac{R^2}{\alpha^2 r^2}, \frac{r^2}{R^2}, \alpha^2\right), \tag{15}$$

and the principal invariants take the form

$$\begin{aligned} I_1 =& \operatorname{tr}(\mathbf{B}) = \frac{R^2}{\alpha^2 r^2} + \frac{r^2}{R^2} + \alpha^2, \\ I_2 =& \frac{1}{2}\left[(\operatorname{tr}\mathbf{B})^2 - \operatorname{tr}\left(\mathbf{B}^2\right)\right] = \frac{\alpha^2 r^2}{R^2} + \frac{R^2}{r^2} + \frac{1}{\alpha^2}, \\ I_3 =& \det \mathbf{B} = 1. \end{aligned} \tag{16}$$

The principal components of the equilibrium Cauchy stress tensor at time t are

$$\begin{aligned} T^{(0)}_{rr} &= -p^{(0)} + \beta_1 \frac{R^2}{\alpha^2 r^2} + \beta_{-1} \frac{\alpha^2 r^2}{R^2}, \\ T^{(0)}_{\theta\theta} &= T^{(0)}_{rr} + \left(\beta_1 - \beta_{-1}\alpha^2\right)\left(\frac{r^2}{R^2} - \frac{R^2}{\alpha^2 r^2}\right), \\ T^{(0)}_{zz} &= T^{(0)}_{rr} + \left(\beta_1 - \beta_{-1}\frac{r^2}{R^2}\right)\left(\alpha^2 - \frac{R^2}{\alpha^2 r^2}\right), \end{aligned} \tag{17}$$

where $p^{(0)}$ is the Lagrangian multiplier for the incompressibility constraint ($I_3 = 1$), and

$$\beta_1 = 2\frac{\partial W}{\partial I_1}, \qquad \beta_{-1} = -2\frac{\partial W}{\partial I_2} \tag{18}$$

are the nonlinear material parameters, with I_1 and I_2 given by (16).

As the stress components depend only on the radius r, the system of equilibrium equations reduces to

$$\frac{\partial T^{(0)}_{rr}}{\partial r} = \frac{T^{(0)}_{\theta\theta} - T^{(0)}_{rr}}{r}. \tag{19}$$

Hence, by (17) and (19), the radial Cauchy stress for the equilibrium state at time t takes the form

$$T^{(0)}_{rr}(r,t) = \int \left(\beta_1 - \beta_{-1}\alpha^2\right)\left(\frac{r^2}{R^2} - \frac{R^2}{\alpha^2 r^2}\right)\frac{\mathrm{d}r}{r} + \psi(t), \tag{20}$$

where $\psi = \psi(t)$ is an arbitrary function of time. Substitution of (13) and (20) into (10) then gives the principal Cauchy stress components at time t as follows,

$$\begin{aligned} T_{rr}(r,t) &= \rho\left(a\ddot{a}\log r + \dot{a}^2 \log r + \frac{a^2\dot{a}^2}{2r^2}\right) + \int \left(\beta_1 - \beta_{-1}\alpha^2\right)\left(\frac{r^2}{R^2} - \frac{R^2}{\alpha^2 r^2}\right)\frac{\mathrm{d}r}{r} + \psi(t), \\ T_{\theta\theta}(r,t) &= T_{rr}(r,t) + \left(\beta_1 - \beta_{-1}\alpha^2\right)\left(\frac{r^2}{R^2} - \frac{R^2}{\alpha^2 r^2}\right), \\ T_{zz}(r,t) &= T_{rr}(r,t) + \left(\beta_1 - \beta_{-1}\frac{r^2}{R^2}\right)\left(\alpha^2 - \frac{R^2}{\alpha^2 r^2}\right). \end{aligned} \tag{21}$$

3.2 Oscillatory motion of a tube with two stochastic neo-Hookean phases

To study explicitly the behaviour under the quasi-equilibrated radial motion of a composite formed from two concentric homogeneous cylindrical tubes (see Figure 1), we focus on composite tubes with two stochastic neo-Hookean phases. We define the following strain-energy function,

$$\mathcal{W}(\lambda_1,\lambda_2,\lambda_3)=\begin{cases}\frac{\mu^{(1)}}{2}\left(\lambda_1^2+\lambda_2^2+\lambda_3^2-3\right), & C<R<A,\\ \frac{\mu^{(2)}}{2}\left(\lambda_1^2+\lambda_2^2+\lambda_3^2-3\right), & A<R<B,\end{cases} \tag{22}$$

where $C<R<A$ and $A<R<B$ denote the radii of the inner and outer tube in the reference configuration, respectively, and the corresponding shear moduli $\mu^{(1)}$ and $\mu^{(2)}$ are (spatially-independent) random variables characterised by the Gamma distributions $g(u;\rho_1^{(1)},\rho_2^{(1)})$ and $g(u;\rho_1^{(2)},\rho_2^{(2)})$, defined by (4).

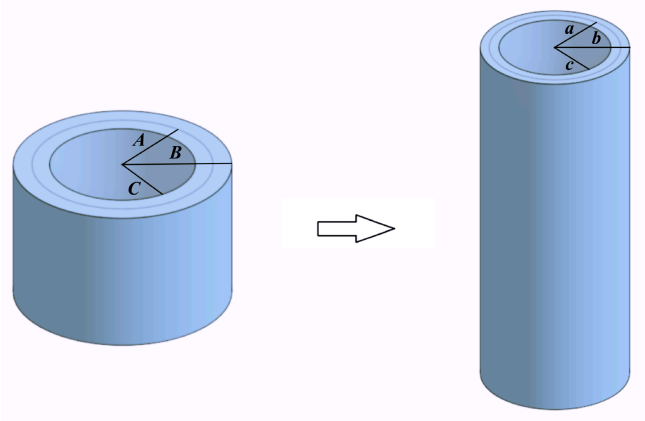

Figure 1: Schematic of a composite cylindrical tube made of two concentric homogeneous tubes, with undeformed outer radii A and B, respectively, showing the reference state (left), and the deformed state, with outer radii a and b of the concentric tubes, respectively (right).

For the deformed composite tube, we denote the radial pressures acting on the curvilinear surfaces $r=c(t)$ and $r=b(t)$ at time t as $T_1(t)$ and $T_2(t)$, respectively, and impose the continuity condition for the stress components across their interface, $r=a(t)$. Evaluating $T_1(t)=-T_{rr}(c,t)$ and $T_2(t)=-T_{rr}(b,t)$ at $r=c$ and $r=b$, respectively, and subtracting the results, gives

$$\begin{aligned}T_1(t)-T_2(t)=&\frac{\rho}{2}\left[c\ddot{c}\log\frac{b^2}{c^2}+\dot{c}^2\log\frac{b^2}{c^2}+\dot{c}^2\left(\frac{c^2}{b^2}-1\right)\right]\\&+\int_c^a\mu^{(1)}\left(\frac{r^2}{R^2}-\frac{R^2}{\alpha^2r^2}\right)\frac{\mathrm{d}r}{r}+\int_a^b\mu^{(2)}\left(\frac{r^2}{R^2}-\frac{R^2}{\alpha^2r^2}\right)\frac{\mathrm{d}r}{r}.\\=&\frac{\rho C^2}{2}\left[\left(\frac{c}{C}\frac{\ddot{c}}{C}+\frac{\dot{c}^2}{C^2}\right)\log\frac{b^2}{c^2}+\frac{\dot{c}^2}{C^2}\left(\frac{c^2}{b^2}-1\right)\right]\\&+\int_c^a\mu^{(1)}\left(\frac{r^2}{R^2}-\frac{R^2}{\alpha^2r^2}\right)\frac{\mathrm{d}r}{r}+\int_a^b\mu^{(2)}\left(\frac{r^2}{R^2}-\frac{R^2}{\alpha^2r^2}\right)\frac{\mathrm{d}r}{r}.\end{aligned} \tag{23}$$

We set the notation

$$u=\frac{r^2}{R^2}=\frac{r^2}{\alpha\left(r^2-c^2\right)+C^2},\qquad x=\frac{c}{C},\qquad \gamma=\frac{B^2}{C^2}-1, \tag{24}$$

and rewrite

$$\begin{aligned}\left(\frac{c}{C}\frac{\ddot{c}}{C}+\frac{\dot{c}^2}{C^2}\right)\log\frac{b^2}{c^2}+\frac{\dot{c}^2}{C^2}\left(\frac{c^2}{b^2}-1\right)=&(\ddot{x}x+\dot{x}^2)\log\left(1+\frac{\gamma}{\alpha x^2}\right)-\dot{x}^2\frac{\frac{\gamma}{\alpha x^2}}{1+\frac{\gamma}{\alpha x^2}}\\=&\frac{1}{2}\frac{d}{dx}\left[\dot{x}^2x\log\left(1+\frac{\gamma}{\alpha x^2}\right)\right].\end{aligned} \tag{25}$$

By (11) and (24), we obtain

$$\begin{aligned}
&\int_c^a \mu^{(1)}\left(\frac{r^2}{R^2}-\frac{R^2}{\alpha^2 r^2}\right)\frac{\mathrm{d}r}{r}+\int_a^b \mu^{(2)}\left(\frac{r^2}{R^2}-\frac{R^2}{\alpha^2 r^2}\right)\frac{\mathrm{d}r}{r}\\
=&\int_c^a \mu^{(1)}\left[\frac{r^2}{\alpha(r^2-c^2)+C^2}-\frac{\alpha(r^2-c^2)+C^2}{\alpha^2 r^2}\right]\frac{\mathrm{d}r}{r}\\
&+\int_a^b \mu^{(2)}\left[\frac{r^2}{\alpha(r^2-c^2)+C^2}-\frac{\alpha(r^2-c^2)+C^2}{\alpha^2 r^2}\right]\frac{\mathrm{d}r}{r}\\
=&-\frac{1}{2}\int_{c^2/C^2}^{a^2/A^2}\mu^{(1)}\frac{1+\alpha u}{\alpha^2 u^2}\mathrm{d}u-\frac{1}{2}\int_{a^2/A^2}^{b^2/B^2}\mu^{(2)}\frac{1+\alpha u}{\alpha^2 u^2}\mathrm{d}u\\
=&\frac{1}{2}\int_{\frac{C^2}{A^2}\left(x^2-\frac{1}{\alpha}\right)+\frac{1}{\alpha}}^{x^2}\mu^{(1)}\frac{1+\alpha u}{\alpha^2 u^2}\mathrm{d}u+\frac{1}{2}\int_{\frac{x^2+\frac{\gamma}{\alpha}}{1+\gamma}}^{\frac{C^2}{A^2}\left(x^2-\frac{1}{\alpha}\right)+\frac{1}{\alpha}}\mu^{(2)}\frac{1+\alpha u}{\alpha^2 u^2}\mathrm{d}u.
\end{aligned}\tag{26}$$

In the above calculations, we used the following relations,

$$r=\left[\frac{u(C^2-\alpha c^2)}{1-\alpha u}\right]^{1/2},\tag{27}$$

$$\frac{\mathrm{d}r}{\mathrm{d}u}=\frac{C^2-\alpha c^2}{2\left(1-\alpha u\right)^2}\left[\frac{u(C^2-\alpha c^2)}{1-\alpha u}\right]^{-1/2}=\frac{r}{2u(1-\alpha u)},\tag{28}$$

$$\left(u-\frac{1}{\alpha^2 u}\right)\frac{1}{2u(1-\alpha u)}=\frac{\alpha^2u^2-1}{2\alpha^2u^2(1-\alpha u)}=-\frac{1+\alpha u}{2\alpha^2u^2}.\tag{29}$$

We then express equation (23) equivalently as follows,

$$\begin{aligned}
2x\frac{T_1(t)-T_2(t)}{\rho C^2}=&\frac{1}{2}\frac{d}{dx}\left[\dot{x}^2x^2\log\left(1+\frac{\gamma}{\alpha x^2}\right)\right]\\
&+\frac{x}{\rho C^2}\int_{\frac{C^2}{A^2}\left(x^2-\frac{1}{\alpha}\right)+\frac{1}{\alpha}}^{x^2}\mu^{(1)}\frac{1+\alpha u}{\alpha^2u^2}\mathrm{d}u\\
&+\frac{x}{\rho C^2}\int_{\frac{x^2+\frac{\gamma}{\alpha}}{1+\gamma}}^{\frac{C^2}{A^2}\left(x^2-\frac{1}{\alpha}\right)+\frac{1}{\alpha}}\mu^{(2)}\frac{1+\alpha u}{\alpha^2u^2}\mathrm{d}u.
\end{aligned}\tag{30}$$

For the dynamic tube, we define

$$\begin{aligned}
G(x,\gamma)=&\frac{1}{\rho C^2}\int_{\frac{1}{\sqrt{\alpha}}}^{x}\zeta\left[\int_{\zeta^2\frac{C^2}{A^2}+\frac{1}{\alpha}\left(1-\frac{C^2}{A^2}\right)}^{\zeta^2}\mu^{(1)}\frac{1+\alpha u}{\alpha^2u^2}\mathrm{d}u\right]\mathrm{d}\zeta\\
&+\frac{1}{\rho C^2}\int_{\frac{1}{\sqrt{\alpha}}}^{x}\zeta\left[\int_{\frac{\zeta^2+\frac{\gamma}{\alpha}}{1+\gamma}}^{\zeta^2\frac{C^2}{A^2}+\frac{1}{\alpha}\left(1-\frac{C^2}{A^2}\right)}\mu^{(2)}\frac{1+\alpha u}{\alpha^2u^2}\mathrm{d}u\right]\mathrm{d}\zeta.
\end{aligned}\tag{31}$$

This function will be used to establish whether the radial motion of the tube is oscillatory or not.

3.2.1 Composite with two concentric homogeneous tubes subject to impulse traction

We set the pressure impulse (suddenly applied pressure difference)

$$2\alpha\frac{T_1(t)-T_2(t)}{\rho C^2}=\begin{cases}0 & \text{if } t\le 0,\\ p_0 & \text{if } t>0,\end{cases}\tag{32}$$

with p_0 constant in time, and integrating (30) implies

$$\frac{1}{2}\dot{x}^2x^2\log\left(1+\frac{\gamma}{\alpha x^2}\right)+G(x,\gamma)=\frac{p_0}{2\alpha}\left(x^2-\frac{1}{\alpha}\right)+C_0,\tag{33}$$

where $G(x,\gamma)$ is defined by (31) and

$$C_0 = \frac{1}{2}\dot{x}_0^2 x_0^2 \log\left(1+\frac{\gamma}{\alpha x_0^2}\right) + G(x_0,\gamma) - \frac{p_0}{2\alpha}\left(x_0^2 - \frac{1}{\alpha}\right), \tag{34}$$

with the initial conditions $x(0) = x_0$ and $\dot{x}(0) = \dot{x}_0$. From (33), we obtain the velocity

$$\dot{x} = \pm\sqrt{\frac{\frac{p_0}{\alpha}(x^2 - \frac{1}{\alpha}) + 2C_0 - 2G(x,\gamma)}{x^2\log(1+\frac{\gamma}{\alpha x^2})}}. \tag{35}$$

Then, the radial motion is periodic if and only if the equation

$$G(x,\gamma) = \frac{p_0}{2\alpha}\left(x^2 - \frac{1}{\alpha}\right) + C_0 \tag{36}$$

has exactly two distinct solutions, representing the amplitudes of the oscillation, $x = x_1$ and $x = x_2$, such that $0 < x_1 < x_2 < \infty$. By (24), the minimum and maximum radii of the inner surface in the oscillation are equal to $x_1 C$ and $x_2 C$, respectively, and by (35), the period of oscillation is equal to

$$T = 2\left|\int_{x_1}^{x_2}\frac{\mathrm{d}x}{\dot{x}}\right| = 2\left|\int_{x_1}^{x_2}\sqrt{\frac{x^2\log\left(1+\frac{\gamma}{\alpha x^2}\right)}{\frac{p_0}{\alpha}\left(x^2-\frac{1}{\alpha}\right)+2C_0-2G(x,\gamma)}}\mathrm{d}x\right|. \tag{37}$$

For the stochastic composite tube, the amplitude and period of the oscillation are random variables described by probability distributions.

To examine $G(x,\gamma)$ defined by (31), we rewrite this function equivalently as

$$G(x,\gamma) = G_1(x,\gamma) + G_2(x,\gamma), \tag{38}$$

where

$$G_1(x,\gamma) = \frac{1}{\rho C^2}\int_{\frac{1}{\sqrt{\alpha}}}^{x}\zeta\left[\int_{\zeta^2\frac{C^2}{A^2}+\frac{1}{\alpha}\left(1-\frac{C^2}{A^2}\right)}^{\zeta^2}\mu^{(1)}\frac{1+\alpha u}{\alpha^2u^2}\mathrm{d}u\right]\mathrm{d}\zeta \tag{39}$$

and

$$G_2(x,\gamma) = \frac{1}{\rho C^2}\int_{\frac{1}{\sqrt{\alpha}}}^{x}\zeta\left[\int_{\zeta^2}^{\zeta^2\frac{C^2}{A^2}+\frac{1}{\alpha}\left(1-\frac{C^2}{A^2}\right)}\mu^{(2)}\frac{1+\alpha u}{\alpha^2u^2}\mathrm{d}u + \int_{\frac{\zeta^2+\frac{\gamma}{\alpha}}{1+\gamma}}^{\zeta^2}\mu^{(2)}\frac{1+\alpha u}{\alpha^2u^2}\mathrm{d}u\right]\mathrm{d}\zeta. \tag{40}$$

Proceeding as in [42], we obtain

$$G_1(x,\gamma) = \frac{\mu^{(1)}}{2\alpha\rho C^2}\left(\frac{1}{\alpha}-x^2\right)\log\left[\frac{C^2}{A^2}+\frac{1}{\alpha x^2}\left(1-\frac{C^2}{A^2}\right)\right] \tag{41}$$

and

$$G_2(x,\gamma) = \frac{\mu^{(2)}}{2\alpha\rho C^2}\left(x^2-\frac{1}{\alpha}\right)\left\{\log\left[\frac{C^2}{A^2}+\frac{1}{\alpha x^2}\left(1-\frac{C^2}{A^2}\right)\right]+\log\frac{1+\gamma}{1+\frac{\gamma}{\alpha x^2}}\right\}. \tag{42}$$

By (41) and (42), the function $G(x,\gamma)$ defined by (38) takes the form

$$G(x,\gamma) = \frac{1}{2\alpha\rho C^2}\left(x^2-\frac{1}{\alpha}\right)\left\{\left(\mu^{(2)}-\mu^{(1)}\right)\log\left[\frac{C^2}{A^2}+\frac{1}{\alpha x^2}\left(1-\frac{C^2}{A^2}\right)\right]+\mu^{(2)}\log\frac{1+\gamma}{1+\frac{\gamma}{\alpha x^2}}\right\}. \tag{43}$$

This function is monotonically decreasing for $0 < x < 1/\sqrt{\alpha}$ and increasing for $x > 1/\sqrt{\alpha}$. When $\mu^{(1)} = \mu^{(2)}$, the function corresponding to a homogeneous tube is recovered [42].

Assuming that the shear moduli $\mu^{(1)}$ and $\mu^{(2)}$ have a lower bound

$$\mu^{(1)} > \eta, \qquad \mu^{(2)} > \eta, \tag{44}$$

for some constant $\eta > 0$, it follows that

$$\lim_{x\to 0} G(x,\gamma) = \lim_{x\to\infty} G(x,\gamma) = \infty. \tag{45}$$

We consider the following two cases:

(i) If $p_0 = 0$ and $C_0 > 0$, then equation (36) has exactly two solutions, $x = x_1$ and $x = x_2$, satisfying $0 < x_1 < 1/\sqrt{\alpha} < x_2 < \infty$, for any positive constant C_0. Note that these oscillations are not 'free' in general, since, by (21), if $T_{rr}(r,t) = 0$ at $r = c$ and $r = b$, so that $T_1(t) = T_2(t) = 0$, then $T_{\theta\theta}(r,t) \neq 0$ and $T_{zz}(r,t) \neq 0$ at $r = c$ and $r = b$, unless $\alpha \to 1$ and $r^2/R^2 \to 1$ [58]. In Figure 2, we represent the stochastic function $G(x,\gamma)$, defined by (43), intersecting the line $C_0 = 7$, and the associated velocity, given by (35), when $\alpha = 1$, $\rho = 1$, and the shear modulus of the inner phase, $\mu^{(1)}$, follows a Gamma distribution with $\rho_1^{(1)} = 405$ and $\rho_2^{(1)} = 4.05/\rho_1^{(1)} = 0.01$, while the shear modulus of the outer phase, $\mu^{(2)}$, is drawn from a Gamma distribution with $\rho_1^{(2)} = 405$ and $\rho_2^{(2)} = 4.2/\rho_1^{(2)}$.

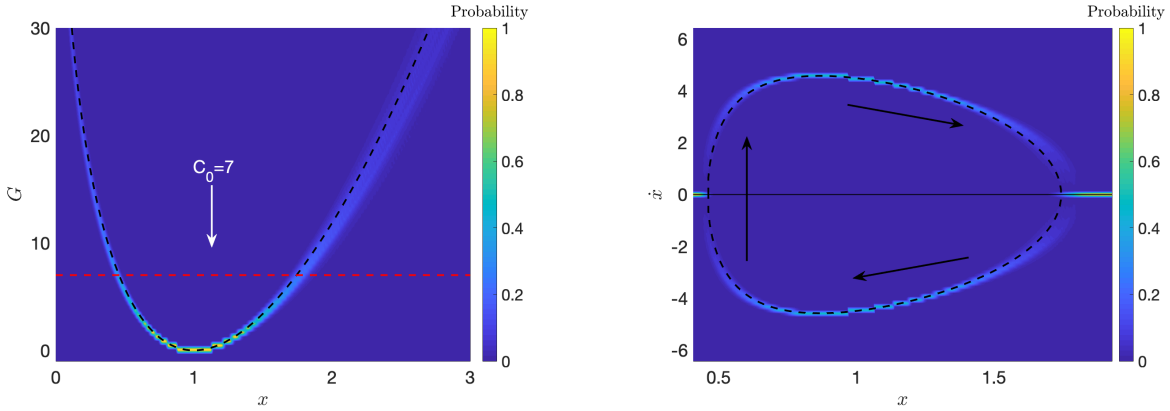

Figure 2: The function $G(x,\gamma)$, defined by (43), intersecting the (dashed red) line $C_0 = 7$ (left), and the associated velocity, given by (35) (right), for a dynamic composite tube with two concentric stochastic neo-Hookean phases, with inner radii $A = 1$ and $C = 1/2$, respectively, assuming that $\alpha = 1$, $\rho = 1$, and $\mu^{(1)}$ follows a Gamma distribution with $\rho_1^{(1)} = 405$ and $\rho_2^{(1)} = 4.05/\rho_1^{(1)} = 0.01$, while $\mu^{(2)}$ is drawn from a Gamma distribution with $\rho_1^{(2)} = 405$ and $\rho_2^{(2)} = 4.2/\rho_1^{(2)}$. The dashed black lines correspond to the expected values based only on mean values, $\underline{\mu}^{(1)} = 4.05$ and $\underline{\mu}^{(2)} = 4.2$. Each distribution was calculated from the average of 1000 stochastic simulations.

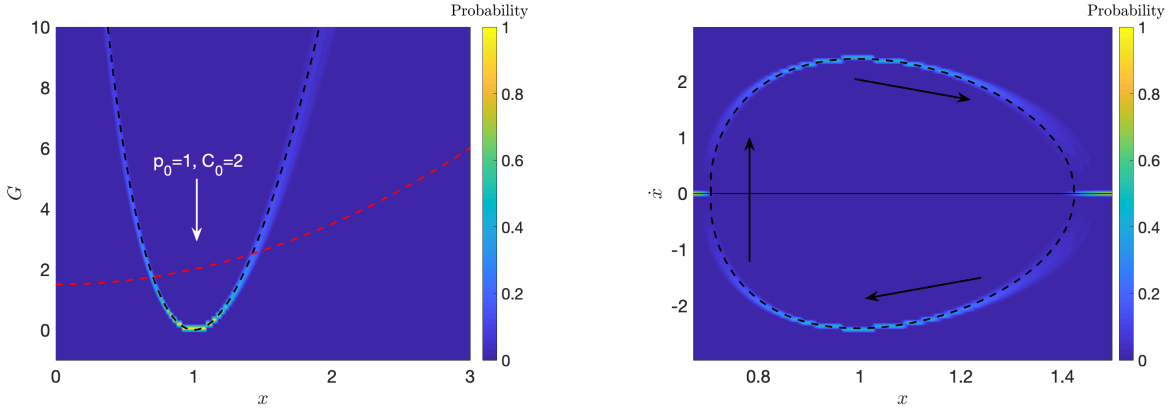

Figure 3: The function $G(x,\gamma)$, defined by (43), intersecting the (dashed red) line $\frac{p_0}{2\alpha}\left(x^2 - \frac{1}{\alpha}\right) + C_0$ when $p_0 = 1$ and $C_0 = 2$ (left), and the associated velocity, given by (35) (right), for a dynamic composite tube with two concentric stochastic neo-Hookean phases, with inner radii $A = 1$ and $C = 1/2$, respectively, under impulse traction, assuming that $\alpha = 1$, $\rho = 1$, and $\mu^{(1)}$ follows a Gamma distribution with $\rho_1^{(1)} = 405$ and $\rho_2^{(1)} = 4.05/\rho_1^{(1)} = 0.01$, while $\mu^{(2)}$ is drawn from a Gamma distribution with $\rho_1^{(2)} = 405$ and $\rho_2^{(2)} = 4.2/\rho_1^{(2)}$. The dashed black lines correspond to the expected values based only on mean values, $\underline{\mu}^{(1)} = 4.05$ and $\underline{\mu}^{(2)} = 4.2$. Each distribution was calculated from the average of 1000 stochastic simulations.

(ii) When $p_0 \neq 0$ and $C_0 \geq 0$, substitution of (43) in (36) gives

$$p_0 = \frac{2\alpha\,(G - C_0)}{x^2 - \frac{1}{\alpha}}. \tag{46}$$

The right-hand side of the above equation is a monotonically increasing function of x, implying that there exists a unique positive x satisfying (46) if and only if the following condition holds,

$$\lim_{x\to 0} \frac{2\alpha\,(G - C_0)}{x^2 - \frac{1}{\alpha}} < p_0 < \lim_{x\to \infty} \frac{2\alpha\,(G - C_0)}{x^2 - \frac{1}{\alpha}}. \tag{47}$$

By (24) and (47), the necessary and sufficient condition that oscillatory motion occurs is that

$$-\infty < p_0 < \frac{\mu^{(1)}}{\rho C^2} \log \frac{A^2}{C^2} + \frac{\mu^{(2)}}{\rho C^2} \log \frac{B^2}{A^2}, \tag{48}$$

where $\mu^{(1)}$ and $\mu^{(2)}$ are described by the Gamma probability density functions $g(u; \rho_1^{(1)}, \rho_2^{(1)})$ and $g(u; \rho_1^{(2)}, \rho_2^{(2)})$, respectively. After rescaling, $\mu^{(1)} \log \frac{A^2}{C^2}$ follows the Gamma distribution with shape parameter $\rho_1^{(1)}$ and scale parameter $\rho_2^{(1)} \log \frac{A^2}{C^2}$ and $\mu^{(2)} \log \frac{B^2}{A^2}$ follows the Gamma distribution with shape parameter $\rho_1^{(2)}$ and scale parameter $\rho_2^{(2)} \log \frac{B^2}{A^2}$. Then, $\mu^{(1)} \log \frac{A^2}{C^2} + \mu^{(2)} \log \frac{B^2}{A^2}$ is a random variable characterised by the sum of the two rescaled Gamma distributions [38, 50]. An example is shown in Figure 3, where $p_0 = 1$ and $C_0 = 2$, while the geometric and material parameters for the composite tube are as in the previous case.

Thin-walled tube. In particular, when the tube wall is thin, such that $0 < \gamma \ll 1$ and $\alpha = 1$, if we assume that $A^2/C^2 = B^2/A^2 = \gamma/2 + 1$, then the problem reduces to that of a thin-walled homogeneous cylindrical tube with shear modulus $\left(\mu^{(1)} + \mu^{(2)}\right)/2$ [42].

3.2.2 Composite with two concentric homogeneous tubes subject to dead-load traction

We now assume that the outer circular surface of the composite tube is free, such that $T_2(t) = 0$, while the inner surface is subject to a dead-load pressure $P_1(t)$ satisfying

$$2\frac{P_1(t)}{\rho C^2} = 2\alpha x \frac{T_1(t)}{\rho C^2} = \begin{cases} 0 & \text{if } t \leq 0, \\ p_0 & \text{if } t > 0, \end{cases} \tag{49}$$

with p_0 constant in time. Integrating (30) implies

$$\frac{1}{2}\dot{x}^2 x^2 \log\left(1 + \frac{\gamma}{\alpha x^2}\right) + G(x, \gamma) = \frac{p_0}{\alpha}\left(x - \frac{1}{\sqrt{\alpha}}\right) + C_0, \tag{50}$$

where $G(x, \gamma)$ is defined by (31) and

$$C_0 = \frac{1}{2}\dot{x}_0^2 x_0^2 \log\left(1 + \frac{\gamma}{\alpha x_0^2}\right) + G(x_0, \gamma) - \frac{p_0}{\alpha}\left(x_0 - \frac{1}{\sqrt{\alpha}}\right), \tag{51}$$

with the initial conditions $x(0) = x_0$ and $\dot{x}(0) = \dot{x}_0$. By (33), the velocity is

$$\dot{x} = \pm\sqrt{\frac{\frac{2p_0}{\alpha}(x - \frac{1}{\sqrt{\alpha}}) + 2C_0 - 2G(x, \gamma)}{x^2 \log(1 + \frac{\gamma}{\alpha x^2})}}. \tag{52}$$

The radial motion is periodic if and only if the equation

$$G(x, \gamma) = \frac{p_0}{\alpha}\left(x - \frac{1}{\sqrt{\alpha}}\right) + C_0 \tag{53}$$

has exactly two distinct solutions, representing the amplitudes of the oscillation, $x = x_1$ and $x = x_2$, such that $0 < x_1 < x_2 < \infty$. By (24), the minimum and maximum radii of the inner surface in the oscillation are equal to $x_1 C$ and $x_2 C$, respectively, and by (35), the period of oscillation is equal to

$$T = 2\left|\int_{x_1}^{x_2} \frac{\mathrm{d}x}{\dot{x}}\right| = 2\left|\int_{x_1}^{x_2} \sqrt{\frac{x^2 \log\left(1+\frac{\gamma}{\alpha x^2}\right)}{\frac{2p_0}{\alpha}\left(x-\frac{1}{\sqrt{\alpha}}\right)+2C_0-2G(x,\gamma)}}\,\mathrm{d}x\right|. \tag{54}$$

For the stochastic composite tube, the amplitude and period of the oscillation are random variables described by probability distributions.

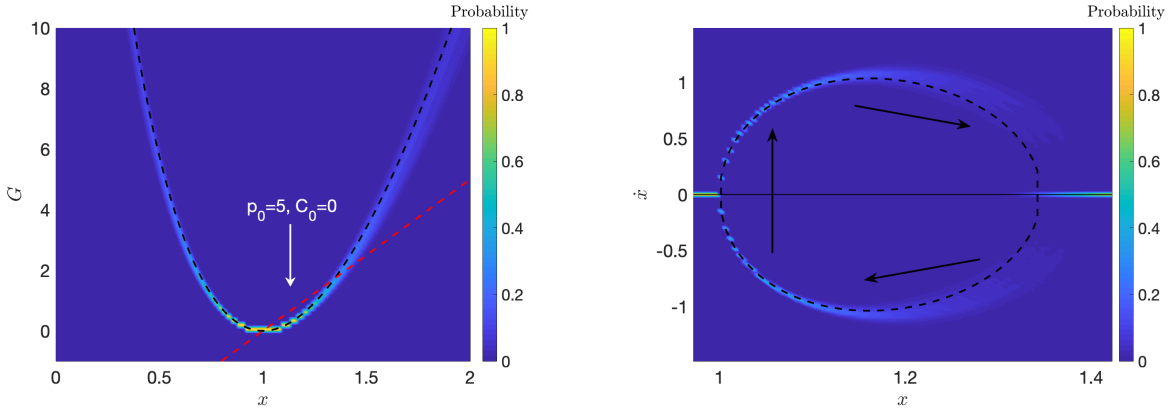

Figure 4: The function $G(x,\gamma)$, defined by (43), intersecting the (dashed red) line $\frac{p_0}{\alpha}\left(x-\frac{1}{\sqrt{\alpha}}\right)+C_0$ when $p_0 = 5$ and $C_0 = 0$ (left), and the associated velocity, given by (35) (right), for a dynamic composite tube with two concentric stochastic neo-Hookean phases, with inner radii $A = 1$ and $C = 1/2$, respectively, under dead-load traction, assuming that $\alpha = 1$, $\rho = 1$, and $\mu^{(1)}$ follows a Gamma distribution with $\rho_1^{(1)} = 405$ and $\rho_2^{(1)} = 4.05/\rho_1^{(1)} = 0.01$, while $\mu^{(2)}$ is drawn from a Gamma distribution with $\rho_1^{(2)} = 405$ and $\rho_2^{(2)} = 4.2/\rho_1^{(2)}$. The dashed black lines correspond to the expected values based only on mean values, $\underline{\mu}^{(1)} = 4.05$ and $\underline{\mu}^{(2)} = 4.2$. Each distribution was calculated from the average of 1000 stochastic simulations.

The case with $p_0 = 0$ is similar to that when an impulse traction was assume. For $p_0 \neq 0$ and $C_0 \geq 0$, substitution of (43) in (53) implies

$$p_0 = \frac{\alpha\,(G - C_0)}{x - \frac{1}{\sqrt{\alpha}}}. \tag{55}$$

The right-hand side of the above equation is a monotonically increasing function of x, implying that there exists a unique positive x satisfying (46) if and only if the following condition holds,

$$-\infty = \lim_{x\to 0} \frac{\alpha\,(G - C_0)}{x - \frac{1}{\sqrt{\alpha}}} < p_0 < \lim_{x\to\infty} \frac{\alpha\,(G - C_0)}{x - \frac{1}{\sqrt{\alpha}}} = \infty. \tag{56}$$

An example is shown in Figure 4, where $p_0 = 5$ and $C_0 = 0$, and the geometric and material parameters for the composite tube are as in the previous case.

3.3 Oscillatory motion of a stochastic radially inhomogeneous tube

We further consider the inflation of a radially inhomogeneous tube of stochastic neo-Hookean-like hyperelastic material characterised by the strain-energy function (1). Intuitively, one can regard the radially inhomogeneous tube as an extension of the composite with two concentric phases to the case with infinitely many concentric layers and continuous inhomogeneity. Our inhomogeneous model is similar to those proposed in [17] where the dynamic inflation of cylindrical tubes and spherical shells

was treated explicitly. Clearly, different models will lead to different results. However, the purpose here is to illustrate our stochastic approach in a mathematically transparent manner by combining it with analytical approaches for the mechanical solution whenever possible.

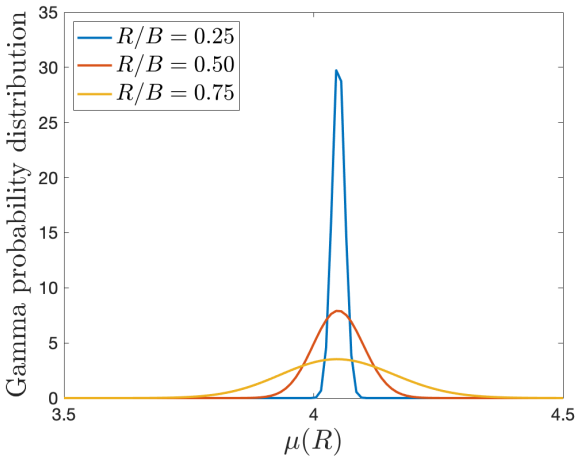

Figure 5: Examples of Gamma distribution, with hyperparameters $\rho_1 = 405 \cdot B^4/R^4$ and $\rho_2 = 0.01 \cdot R^4/B^4$, for the nonlinear shear modulus $\mu(R)$ given by (57).

Specifically, we assume a class of stochastic inhomogeneous hyperelastic models (1) where $\mu = \mu(R)$ takes the form

$$\mu(R) = C_1 + C_2 \frac{R^2}{C^2}, \tag{57}$$

such that $\mu(R) > 0$, for all $C \le R \le B$, $C_1 > 0$ is a single-valued (deterministic) constant, and C_2 is a random value defined by a given probability distribution.

When the mean value of the shear modulus $\mu(R)$ described by (57) does not depend on R, as C_1, R and C are deterministic and C_2 is probabilistic, we have

$$\underline{\mu} = C_1, \qquad \mathrm{Var}[\mu] = \mathrm{Var}[C_2] \frac{R^4}{C^4}, \tag{58}$$

where $\mathrm{Var}[C_2]$ is the variance of C_2, while the mean value of C_2 is $\underline{C}_2 = 0$.

By (3) and (58), the hyperparameters of the corresponding Gamma distribution, defined by (4), take the form

$$\rho_1 = \frac{C_1}{\rho_2}, \qquad \rho_2 = \frac{\mathrm{Var}[\mu]}{C_1} = \frac{\mathrm{Var}[C_2]}{C_1} \frac{R^4}{C^4}. \tag{59}$$

For example, we can choose two constant values, $C_0 > 0$ and $C_1 > 0$, and set the hyperparameters for the Gamma distribution at any given R as follows,

$$\rho_1 = \frac{C_1}{C_0} \frac{C^4}{R^4}, \qquad \rho_2 = C_0 \frac{R^4}{C^4}. \tag{60}$$

By (57), $C_2 = (\mu(R) - C_1)\, C^2/R^2$ is the shifted Gamma-distributed random variable with mean value $\underline{C}_2 = 0$ and variance $\mathrm{Var}[C_2] = \rho_1 \rho_2^2 C^4/R^4 = C_0 C_1$.

In Figure 5, we show Gamma distributions with $\rho_1 = 405 \cdot B^4/R^4$ and $\rho_2 = 0.01 \cdot R^4/B^4$. By (57) and (60), $C_0 = 0.01 \cdot C^4/B^4$, $C_1 = \underline{\mu} = \rho_1 \rho_2 = 4.05$ and $C_2 = \mu(C) - C_1$. In particular, for a tube with infinitely thick wall, as R decreases to C, ρ_1 increases, while ρ_2 decreases, and the Gamma distribution converges to a normal distribution [18, 41].

The shear modulus given by (57) takes the equivalent form

$$\mu(u) = C_1 + C_2 \frac{x^2 - \frac{1}{\alpha}}{u - \frac{1}{\alpha}}, \tag{61}$$

where $u = r^2/R^2$ and $x = c/C$, as denoted in (24).

Next, writing the invariants given by (16) in the equivalent form

$$I_1 = \frac{1}{\alpha^2 u} + u + \alpha^2, \qquad I_2 = \alpha^2 u + \frac{1}{u} + \frac{1}{\alpha^2}, \qquad I_3 = 1, \tag{62}$$

and substituting these in (18) gives

$$\begin{aligned} \beta_1 &= 2\frac{\partial W}{\partial I_1} = \mu + \frac{d\mu}{\mathrm{d}u}\frac{\mathrm{d}u}{\mathrm{d}I_1}\left(I_1 - 3\right), \\ \beta_{-1} &= -2\frac{\partial W}{\partial I_2} = -\frac{\mathrm{d}\mu}{\mathrm{d}u}\frac{\mathrm{d}u}{\mathrm{d}I_2}\left(I_1 - 3\right), \end{aligned} \tag{63}$$

where μ is defined by (61). Therefore,

$$\begin{aligned} \beta_1 &= C_1 + C_2\frac{x^2 - \frac{1}{\alpha}}{u - \frac{1}{\alpha}}\left[1 - \frac{u^3 + u^2\left(\alpha^2 - 3\right) + \frac{u}{\alpha^2}}{\left(u - \frac{1}{\alpha}\right)^2\left(u + \frac{1}{\alpha}\right)}\right], \\ \beta_{-1} &= C_2\frac{x^2 - \frac{1}{\alpha}}{u - \frac{1}{\alpha}}\frac{\frac{u^3}{\alpha^2} + u^2\left(1 - \frac{3}{\alpha^2}\right) + \frac{u}{\alpha^4}}{\left(u - \frac{1}{\alpha}\right)^2\left(u + \frac{1}{\alpha}\right)}, \end{aligned} \tag{64}$$

and

$$\beta_1 - \beta_{-1}\alpha^2 = C_1 + 2C_2\frac{x^2 - \frac{1}{\alpha}}{u - \frac{1}{\alpha}}\left[\frac{1}{2} - \frac{u^3 + u^2\left(\alpha^2 - 3\right) + \frac{u}{\alpha^2}}{\left(u - \frac{1}{\alpha}\right)^2\left(u + \frac{1}{\alpha}\right)}\right]. \tag{65}$$

Recalling that the stress components are described by (21), and following a similar procedure as in the previous section, we set the pressure impulse as in (32). Then, similarly to (31), using (65), we define the function

$$\begin{aligned} G(x,\gamma) &= \frac{C_1}{\rho C^2}\int_{\frac{1}{\sqrt{\alpha}}}^{x}\left(\zeta\int_{\frac{\zeta^2+\frac{\gamma}{\alpha}}{1+\gamma}}^{\zeta^2}\frac{1+\alpha u}{\alpha^2 u^2}\mathrm{d}u\right)\mathrm{d}\zeta \\ &+ \frac{2C_2}{\rho C^2}\int_{\frac{1}{\sqrt{\alpha}}}^{x}\left\{\left(\zeta^3 - \frac{\zeta}{\alpha}\right)\int_{\frac{\zeta^2+\frac{\gamma}{\alpha}}{1+\gamma}}^{\zeta^2}\frac{1+\alpha u}{\alpha^2 u^2\left(u - \frac{1}{\alpha}\right)}\left[\frac{1}{2} - \frac{u^3 + u^2\left(\alpha^2 - 3\right) + \frac{u}{\alpha^2}}{\left(u - \frac{1}{\alpha}\right)^2\left(u + \frac{1}{\alpha}\right)}\right]\mathrm{d}u\right\}\mathrm{d}\zeta \\ &= \frac{C_1}{2\alpha\rho C^2}\left(x^2 - \frac{1}{\alpha}\right)\log\frac{1+\gamma}{1+\frac{\gamma}{\alpha x^2}} \\ &+ \frac{C_2}{\rho C^2}\int_{\frac{1}{\sqrt{\alpha}}}^{x}\left\{\left(\zeta^3 - \frac{\zeta}{\alpha}\right)\left[\frac{1}{\alpha\zeta^2} - \frac{1+\gamma}{\alpha\zeta^2+\gamma} - \frac{\alpha^3 - 3\alpha + 2}{\left(\alpha\zeta^2 - 1\right)^2} + \frac{\alpha^3 - 3\alpha + 2}{\left(\frac{\alpha\zeta^2+\gamma}{1+\gamma} - 1\right)^2}\right]\right\}\mathrm{d}\zeta. \end{aligned} \tag{66}$$

We restrict our attention on the following limiting cases:

Thick-walled tube. If the tube has an infinitely thick wall, such that $\gamma \to \infty$ and $\alpha = 1$, then (66) takes the form

$$\begin{aligned} G(x) &= \frac{C_1}{\rho C^2}\left(x^2 - 1\right)\log x - \frac{C_2}{\rho C^2}\int_1^x \frac{\left(\zeta^2 - 1\right)^2}{\zeta}\mathrm{d}\zeta \\ &= \frac{C_1}{\rho C^2}\left(x^2 - 1\right)\log x - \frac{C_2}{4\rho C^2}\left(x^4 - 4x^2 + 4\log x + 3\right). \end{aligned} \tag{67}$$

Examples are presented in Figure 6 for the case with no impulse or dead-load traction, in Figure 7 for the case when the pressure impulse is given by (32), and in Figure 8 for the case when the dead-load traction is given by (49).

Thin-walled tube. If the tube wall is thin, such that $0 < \gamma \ll 1$ and $\alpha = 1$, then the shear modulus defined by (57) takes the form $\mu = C_1 + C_2$, and the problem reduces to that of a homogeneous tube with thin wall (see also [42]).

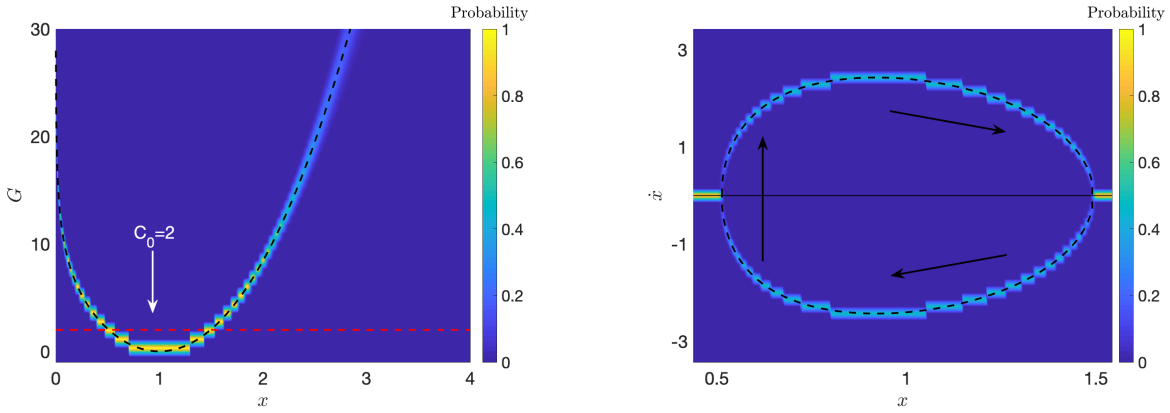

Figure 6: The function $G(x,\gamma)$, defined by (67), intersecting the (dashed red) line $C_0 = 2$ (left), and the associated velocity, given by (35) (right), for a dynamic radially inhomogeneous tube with infinitely thick wall having inner radius $C = 1$, assuming that $\alpha = 1$, $\rho = 1$, and μ follows a Gamma distribution with $\rho_1 = 405/R^4$ and $\rho_2 = 0.01 \cdot R^4$. The dashed black lines correspond to the expected values based only on mean values. Each distribution was calculated from the average of 1000 stochastic simulations.

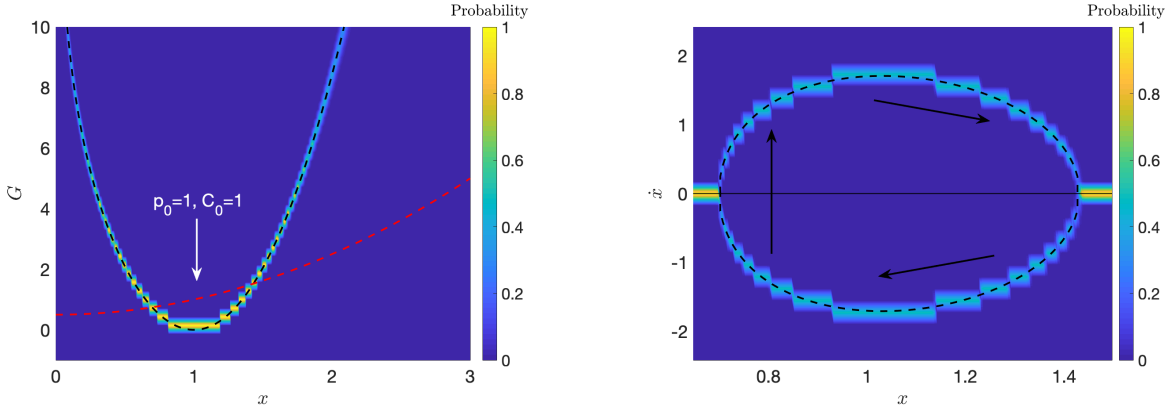

Figure 7: The function $G(x,\gamma)$, defined by (67), intersecting the (dashed red) line $\frac{p_0}{2\alpha}\left(x^2 - \frac{1}{\alpha}\right) + C_0$ when $p_0 = 1$ and $C_0 = 1$ (left), and the associated velocity, given by (35) (right), for a dynamic radially inhomogeneous tube with infinitely thick wall having inner radius $C = 1$ under impulse traction, assuming that $\alpha = 1$, $\rho = 1$, and μ follows a Gamma distribution with $\rho_1 = 405/R^4$ and $\rho_2 = 0.01 \cdot R^4$. The dashed black lines correspond to the expected values based only on mean values. Each distribution was calculated from the average of 1000 stochastic simulations.

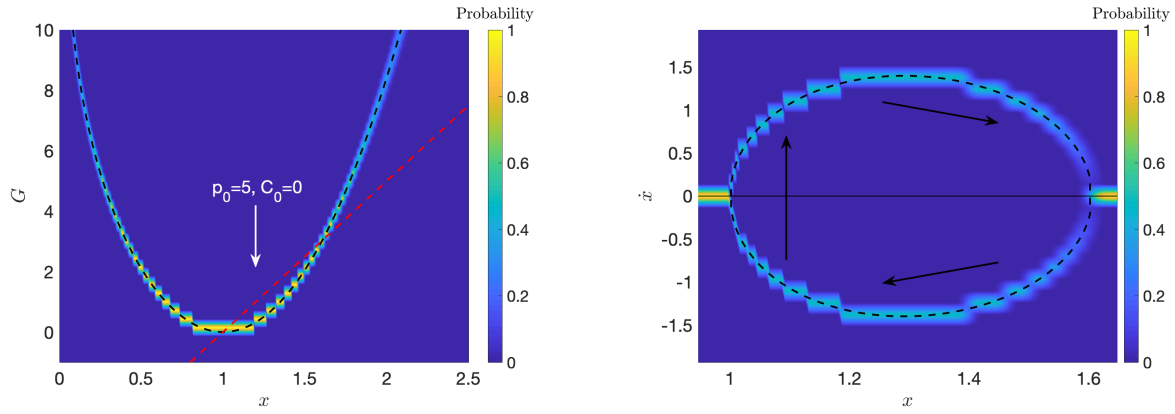

Figure 8: The function $G(x,\gamma)$, defined by (67), intersecting the (dashed red) line $\frac{p_0}{\alpha}\left(x-\frac{1}{\sqrt{\alpha}}\right)+C_0$ when $p_0=5$ and $C_0=0$ (left), and the associated velocity, given by (35) (right), for a dynamic radially inhomogeneous tube with infinitely thick wall having inner radius $C=1$ under dead-load traction, assuming that $\alpha=1$, $\rho=1$, and μ follows a Gamma distribution with $\rho_1=405/R^4$ and $\rho_2=0.01\cdot R^4$. The dashed black lines correspond to the expected values based only on mean values. Each distribution was calculated from the average of 1000 stochastic simulations.

4 Quasi-equilibrated motion of stochastic spherical shells

Next, we analyse the oscillatory motion of two concentric homogeneous spherical shells and of a radially inhomogeneous shell with stochastic constitutive parameters.

4.1 Radial motion of a spherical shell

For a spherical shell, the radial motion is described by [6, 9, 26, 36]

$$r^3=c^3+R^3-C^3,\qquad \theta=\Theta,\qquad \phi=\Phi, \tag{68}$$

where (R,Θ,Φ) and (r,θ,ϕ) are the spherical polar coordinates in the reference and current configuration, respectively, such that $C\leq R\leq B$, C and B are the inner and outer radii in the undeformed state, and $c=c(t)$ and $b=b(t)=\sqrt[3]{c^3+B^3-C^3}$ are the inner and outer radii at time t, respectively.

As for the cylindrical tube, the radial motion (68) of the spherical shell is determined entirely by the inner radius c at time t. By the governing equations (68), condition (9) is valid for $\mathbf{x}=(r,\theta,\phi)^T$. Hence, (68) describes a quasi-equilibrated motion, such that

$$-\frac{\partial\xi}{\partial r}=\ddot{r}=\frac{2c\dot{c}^2+c^2\ddot{c}}{r^2}-\frac{2a^4\dot{c}^2}{r^5}, \tag{69}$$

where ξ is the acceleration potential satisfying (8). Integrating (69) gives [75, p. 217]

$$-\xi=-\frac{2c\dot{c}^2+a^2\ddot{c}}{r}+\frac{c^4\dot{c}^2}{2r^4}=-r\ddot{r}-\frac{3}{2}\dot{r}^2. \tag{70}$$

For the deformation (68), the gradient tensor with respect to the polar coordinates (R,Θ,Φ) takes the form

$$\mathbf{F}=\operatorname{diag}\left(\frac{R^2}{r^2},\frac{r}{R},\frac{r}{R}\right), \tag{71}$$

the Cauchy-Green tensor is equal to

$$\mathbf{B}=\mathbf{F}^2=\operatorname{diag}\left(\frac{R^4}{r^4},\frac{r^2}{R^2},\frac{r^2}{R^2}\right), \tag{72}$$

and the corresponding principal invariants are

$$\begin{aligned} I_1 =& \text{tr } (\mathbf{B}) = \frac{R^4}{r^4} + 2\frac{r^2}{R^2}, \\ I_2 =& \frac{1}{2}\left[(\text{tr}\,\mathbf{B})^2 - \text{tr}\left(\mathbf{B}^2\right)\right] = \frac{r^4}{R^4} + 2\frac{R^2}{r^2}, \\ I_3 =& \det \mathbf{B} = 1. \end{aligned} \tag{73}$$

Then, the principal components of the equilibrium Cauchy stress at time t are

$$\begin{aligned} T^{(0)}_{rr} &= -p^{(0)} + \beta_1 \frac{R^4}{r^4} + \beta_{-1}\frac{r^4}{R^4}, \\ T^{(0)}_{\theta\theta} &= T^{(0)}_{rr} + \left(\beta_1 - \beta_{-1}\frac{r^2}{R^2}\right)\left(\frac{r^2}{R^2} - \frac{R^4}{r^4}\right), \\ T^{(0)}_{\phi\phi} &= T^{(0)}_{\theta\theta}, \end{aligned} \tag{74}$$

where $p^{(0)}$ is the Lagrangian multiplier for the incompressibility constraint ($I_3 = 1$), and

$$\beta_1 = 2\frac{\partial W}{\partial I_1}, \qquad \beta_{-1} = -2\frac{\partial W}{\partial I_2}, \tag{75}$$

with I_1 and I_2 given by (73).

As the stress components depend only on the radius r, the system of equilibrium equations reduces to

$$\frac{\partial T^{(0)}_{rr}}{\partial r} = 2\frac{T^{(0)}_{\theta\theta} - T^{(0)}_{rr}}{r}. \tag{76}$$

Hence, by (74) and (76), the radial Cauchy stress for the equilibrium state at t is equal to

$$T^{(0)}_{rr}(r,t) = 2\int \left(\beta_1 - \beta_{-1}\frac{r^2}{R^2}\right)\left(\frac{r^2}{R^2} - \frac{R^4}{r^4}\right)\frac{\mathrm{d}r}{r} + \psi(t), \tag{77}$$

where $\psi = \psi(t)$ is an arbitrary function of time. Substitution of (70) and (77) into (10) gives the following principal Cauchy stresses at time t,

$$\begin{aligned} T_{rr}(r,t) &= -\rho\left(\frac{c^2\ddot{c} + 2c\dot{c}^2}{r} - \frac{c^4\dot{c}^2}{2r^4}\right) + 2\int \left(\beta_1 - \beta_{-1}\frac{r^2}{R^2}\right)\left(\frac{r^2}{R^2} - \frac{R^4}{r^4}\right)\frac{\mathrm{d}r}{r} + \psi(t), \\ T_{\theta\theta}(r,t) &= T_{rr}(r,t) + \left(\beta_1 - \beta_{-1}\frac{r^2}{R^2}\right)\left(\frac{r^2}{R^2} - \frac{R^4}{r^4}\right), \\ T_{\phi\phi}(r,t) &= T_{\theta\theta}(r,t). \end{aligned} \tag{78}$$

4.2 Oscillatory motion of a spherical shell with two stochastic neo-Hookean phases

We are interested in the behaviour under quasi-equilibrated radial motion of a composite formed from two stochastic neo-Hookean phases, similar to those containing two concentric spheres of different neo-Hookean material treated deterministically in [27] and [61], and stochastically in [49] (see Figure 9). We define the following strain-energy function,

$$\mathcal{W}(\lambda_1,\lambda_2,\lambda_3) = \begin{cases} \frac{\mu^{(1)}}{2}\left(\lambda_1^2 + \lambda_2^2 + \lambda_3^2 - 3\right), & C < R < A, \\ \frac{\mu^{(2)}}{2}\left(\lambda_1^2 + \lambda_2^2 + \lambda_3^2 - 3\right), & A < R < B, \end{cases} \tag{79}$$

where $C < R < A$ and $A < R < B$ denote the radii of the inner and outer sphere in the reference configuration, and the corresponding shear moduli $\mu^{(1)}$ and $\mu^{(2)}$ are (spatially-independent) random variables characterised by the Gamma distributions $g(u;\rho_1^{(1)},\rho_2^{(1)})$ and $g(u;\rho_1^{(2)},\rho_2^{(2)})$, respectively.

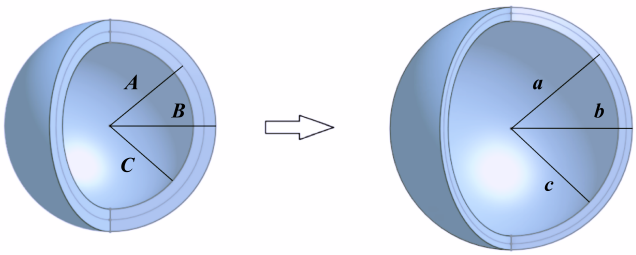

Figure 9: Schematic of a composite spherical shell made of two concentric homogeneous shells, with undeformed outer radii A and B, respectively, showing the reference state (left), and the deformed state, with outer radii a and b of the concentric shells, respectively (right).

For the spherical shell deforming by (68), we set the inner and outer radial pressures acting on the curvilinear surfaces, $r = c(t)$ and $r = b(t)$ at time t, as $T_1(t)$ and $T_2(t)$, respectively [75, pp. 217-219]. Then, evaluating $T_1(t) = -T_{rr}(c,t)$ and $T_2(t) = -T_{rr}(b,t)$, using (78), with $r = c$ and $r = b$, respectively, and subtracting the results, gives

$$\begin{aligned}
T_1(t) - T_2(t) &= \rho\left[\left(c^2\ddot{c} + 2c\dot{c}^2\right)\left(\frac{1}{c} - \frac{1}{b}\right) - \frac{c^4\dot{c}^2}{2}\left(\frac{1}{c^4} - \frac{1}{b^4}\right)\right] \\
&\quad + 2\int_c^a \mu^{(1)}\left(\frac{r^2}{R^2} - \frac{R^4}{r^4}\right)\frac{\mathrm{d}r}{r} + 2\int_a^b \mu^{(2)}\left(\frac{r^2}{R^2} - \frac{R^4}{r^4}\right)\frac{\mathrm{d}r}{r} \\
&= \rho\left[\left(c\ddot{c} + 2\dot{c}^2\right)\left(1 - \frac{c}{b}\right) - \frac{\dot{c}^2}{2}\left(1 - \frac{c^4}{b^4}\right)\right] \\
&\quad + 2\int_c^a \mu^{(1)}\left(\frac{r^2}{R^2} - \frac{R^4}{r^4}\right)\frac{\mathrm{d}r}{r} + 2\int_a^b \mu^{(2)}\left(\frac{r^2}{R^2} - \frac{R^4}{r^4}\right)\frac{\mathrm{d}r}{r} \\
&= \rho C^2\left[\left(\frac{c}{C}\frac{\ddot{c}}{C} + 2\frac{\dot{c}^2}{C^2}\right)\left(1 - \frac{c}{b}\right) - \frac{\dot{c}^2}{2C^2}\left(1 - \frac{c^4}{b^4}\right)\right] \\
&\quad + 2\int_c^a \mu^{(1)}\left(\frac{r^2}{R^2} - \frac{R^4}{r^4}\right)\frac{\mathrm{d}r}{r} + 2\int_a^b \mu^{(2)}\left(\frac{r^2}{R^2} - \frac{R^4}{r^4}\right)\frac{\mathrm{d}r}{r}.
\end{aligned} \tag{80}$$

Setting the notation

$$u = \frac{r^3}{R^3} = \frac{r^3}{r^3 - c^3 + C^3}, \qquad x = \frac{c}{C}, \qquad \gamma = \frac{B^3}{C^3} - 1, \tag{81}$$

we rewrite

$$\begin{aligned}
&\left(\frac{c}{C}\frac{\ddot{c}}{C} + 2\frac{\dot{c}^2}{C^2}\right)\left(1 - \frac{c}{b}\right) - \frac{\dot{a}^2}{2A^2}\left(1 - \frac{a^4}{b^4}\right) \\
&\qquad = \left(\ddot{x}x + 2\dot{x}^2\right)\left[1 - \left(1 + \frac{\gamma}{x^3}\right)^{-1/3}\right] - \frac{\dot{x}^2}{2}\left[1 - \left(1 + \frac{\gamma}{x^3}\right)^{-4/3}\right] \\
&\qquad = \left(\ddot{x}x + \frac{3}{2}\dot{x}^2\right)\left[1 - \left(1 + \frac{\gamma}{x^3}\right)^{-1/3}\right] - \frac{\dot{x}^2}{2}\frac{\gamma}{x^3}\left(1 + \frac{\gamma}{x^3}\right)^{-4/3} \\
&\qquad = \frac{1}{2x^2}\frac{d}{dx}\left\{\dot{x}^2x^3\left[1 - \left(1 + \frac{\gamma}{x^3}\right)^{-1/3}\right]\right\}.
\end{aligned}$$

By (68) and (81), we obtain

$$\begin{aligned}
&\int_c^a \mu^{(1)} \left(\frac{r^2}{R^2} - \frac{R^4}{r^4}\right) \frac{\mathrm{d}r}{r} + \int_a^b \mu^{(2)} \left(\frac{r^2}{R^2} - \frac{R^4}{r^4}\right) \frac{\mathrm{d}r}{r} \\
&= \int_c^a \mu^{(1)} \left[\left(\frac{r^3}{r^3 - c^3 + C^3}\right)^{2/3} - \left(\frac{r^3 - c^3 + C^3}{r^3}\right)^{4/3}\right] \frac{\mathrm{d}r}{r} \\
&+ \int_a^b \mu^{(2)} \left[\left(\frac{r^3}{r^3 - c^3 + C^3}\right)^{2/3} - \left(\frac{r^3 - c^3 + C^3}{r^3}\right)^{4/3}\right] \frac{\mathrm{d}r}{r} \\
&= -\frac{1}{3} \int_{c^3/C^3}^{a^3/A^3} \mu^{(1)} \frac{1+u}{u^{7/3}} \mathrm{d}u - \frac{1}{3} \int_{a^3/A^3}^{b^3/B^3} \mu^{(2)} \frac{1+u}{u^{7/3}} \mathrm{d}u \\
&= \frac{1}{3} \int_{\frac{C^3}{A^3}(x^3-1)+1}^{x^3} \mu^{(1)} \frac{1+u}{u^{7/3}} \mathrm{d}u + \frac{1}{3} \int_{\frac{x^3+\gamma}{1+\gamma}}^{\frac{C^3}{A^3}(x^3-1)+1} \mu^{(2)} \frac{1+u}{u^{7/3}} \mathrm{d}u.
\end{aligned}$$

In the above calculations, we used the following relations,

$$r = \left[\frac{u(C^3 - c^3)}{1-u}\right]^{1/3}, \tag{82}$$

$$\frac{\mathrm{d}r}{\mathrm{d}u} = \frac{C^3 - c^3}{3\,(1-u)^2} \left[\frac{u(C^3 - c^3)}{1-u}\right]^{-2/3} = \frac{r}{3u(1-u)}, \tag{83}$$

$$\left(u^{2/3} - \frac{1}{u^{4/3}}\right) \frac{1}{3u(1-u)} = \frac{u^2 - 1}{3u^2(1-u)} = -\frac{1+u}{3u^{7/3}}. \tag{84}$$

We then express (80) equivalently as follows

$$\begin{aligned}
2x^2 \frac{T_1(t) - T_2(t)}{\rho C^2} &= \frac{d}{dx} \left\{\dot{x}^2 x^3 \left[1 - \left(1 + \frac{\gamma}{x^3}\right)^{-1/3}\right]\right\} \\
&+ \frac{4x^2}{3\rho C^2} \int_{\frac{C^3}{A^3}(x^3-1)+1}^{x^3} \mu^{(1)} \frac{1+u}{u^{7/3}} \mathrm{d}u \\
&+ \frac{4x^2}{3\rho C^2} \int_{\frac{x^3+\gamma}{1+\gamma}}^{\frac{C^3}{A^3}(x^3-1)+1} \mu^{(2)} \frac{1+u}{u^{7/3}} \mathrm{d}u.
\end{aligned} \tag{85}$$

For the dynamic shell, we define

$$H(x,\gamma) = \frac{4}{3\rho C^2} \int_1^x \zeta^2 \left[\int_{\frac{C^3}{A^3}(\zeta^3-1)+1}^{\zeta^3} \mu^{(1)} \frac{1+u}{u^{7/3}} \mathrm{d}u + \int_{\frac{\zeta^3+\gamma}{1+\gamma}}^{\frac{C^3}{A^3}(\zeta^3-1)+1} \mu^{(2)} \frac{1+u}{u^{7/3}} \mathrm{d}u\right] \mathrm{d}\zeta. \tag{86}$$

This function will be used to establish whether the radial motion of the composite shell is oscillatory or not.

4.2.1 Composite with two concentric homogeneous spherical shells subject to impulse traction

Setting the pressure impulse

$$2\frac{T_1(t) - T_2(t)}{\rho C^2} = \begin{cases} 0 & \text{if } t \le 0, \\ p_0 & \text{if } t > 0, \end{cases} \tag{87}$$

with p_0 constant in time, and integrating (85) implies

$$\dot{x}^2 x^3 \left[1 - \left(1 + \frac{\gamma}{x^3}\right)^{-1/3}\right] + H(x,\gamma) = \frac{p_0}{3}\left(x^3 - 1\right) + C_0, \tag{88}$$

where $H(x,\gamma)$ is given by (86), and

$$C_0 = \dot{x}_0^2 x_0^3 \left[1 - \left(1 + \frac{\gamma}{x_0^3}\right)^{-1/3}\right] + H(x_0,\gamma) - \frac{p_0}{3}\left(x_0^3 - 1\right), \tag{89}$$

with the initial conditions $x(0) = x_0$ and $\dot{x}(0) = \dot{x}_0$. By (88), the velocity is equal to

$$\dot{x} = \pm\sqrt{\frac{\frac{p_0}{3}\left(x^3-1\right) + C_0 - H(x,\gamma)}{x^3\left[1 - \left(1+\frac{\gamma}{x^3}\right)^{-1/3}\right]}}. \tag{90}$$

Oscillatory motion of the composite spherical shell is obtained if and only if the equation

$$H(x,\gamma) = \frac{p_0}{3}\left(x^3 - 1\right) + C_0, \tag{91}$$

has exactly two distinct solutions, representing the amplitudes of the oscillation, $x = x_1$ and $x = x_2$, such that $0 < x_1 < x_2 < \infty$. In this case, the minimum and maximum radii of the inner surface in the oscillation are given by $x_1 A$ and $x_2 A$, respectively, and the period of oscillation is equal to

$$T = 2\left|\int_{x_1}^{x_2} \frac{\mathrm{d}x}{\dot{x}}\right| = 2\left|\int_{x_1}^{x_2} \sqrt{\frac{x^3\left[1 - \left(1+\frac{\gamma}{x^3}\right)^{-1/3}\right]}{\frac{p_0}{3}\left(x^3-1\right) + C_0 - H(x,\gamma)}}\mathrm{d}x\right|. \tag{92}$$

For the stochastic composite shell, the amplitude and period of the oscillation are random variables characterised by probability distributions.

To examine $H(x,\gamma)$ defined by (86), we rewrite this function in the equivalent form

$$H(x,\gamma) = H_1(x,\gamma) + H_2(x,\gamma), \tag{93}$$

where

$$H_1(x,\gamma) = \frac{4\mu^{(1)}}{3\rho C^2}\int_1^x \zeta^2\left[\int_{\frac{C^3}{A^3}(\zeta^3-1)+1}^{\zeta^3} \frac{1+u}{u^{7/3}}\mathrm{d}u\right]\mathrm{d}\zeta, \tag{94}$$

and

$$H_2(x,\gamma) = \frac{4\mu^{(2)}}{3\rho C^2}\int_1^x \zeta^2\left[\int_{\zeta^3}^{\frac{C^3}{A^3}(\zeta^3-1)+1} \frac{1+u}{u^{7/3}}\mathrm{d}u + \int_{\frac{\zeta^3+\gamma}{1+\gamma}}^{\zeta^3} \frac{1+u}{u^{7/3}}\mathrm{d}u\right]\mathrm{d}\zeta. \tag{95}$$

Proceeding as in [42], we obtain

$$\begin{aligned} H_1(x,\gamma) = {} & \frac{\mu^{(1)}}{\rho C^2}\left(x^3-1\right)\frac{2x^3-1}{x^3+x^2+x} \\ & - \frac{\mu^{(1)}}{\rho C^2}\left(x^3-1\right)\frac{2\left[\frac{C^3}{A^3}\left(x^3-1\right)+1\right]-1}{\left[\frac{C^3}{A^3}\left(x^3-1\right)+1\right] + \left[\frac{C^3}{A^3}\left(x^3-1\right)+1\right]^{2/3} + \left[\frac{C^3}{A^3}\left(x^3-1\right)+1\right]^{1/3}} \end{aligned} \tag{96}$$

and

$$\begin{aligned} H_2(x,\gamma) = {} & \frac{\mu^{(2)}}{\rho C^2}\left(x^3-1\right)\frac{2\left[\frac{C^3}{A^3}\left(x^3-1\right)+1\right]-1}{\left[\frac{C^3}{A^3}\left(x^3-1\right)+1\right] + \left[\frac{C^3}{A^3}\left(x^3-1\right)+1\right]^{2/3} + \left[\frac{C^3}{A^3}\left(x^3-1\right)+1\right]^{1/3}} \\ & - \frac{\mu^{(2)}}{\rho C^2}\left(x^3-1\right)\frac{2\frac{x^3+\gamma}{1+\gamma}-1}{\frac{x^3+\gamma}{1+\gamma} + \left(\frac{x^3+\gamma}{1+\gamma}\right)^{2/3} + \left(\frac{x^3+\gamma}{1+\gamma}\right)^{1/3}}. \end{aligned} \tag{97}$$

By (96) and (97), the function $H(x,\gamma)$ defined by (93) takes the form

$$\begin{aligned} H(x,\gamma) &= \frac{\mu^{(1)}}{\rho C^2}\left(x^3-1\right)\frac{2x^3-1}{x^3+x^2+x} \\ &+ \frac{\mu^{(2)}-\mu^{(1)}}{\rho C^2}\left(x^3-1\right)\frac{2\left[\frac{C^3}{A^3}\left(x^3-1\right)+1\right]-1}{\left[\frac{C^3}{A^3}\left(x^3-1\right)+1\right]+\left[\frac{C^3}{A^3}\left(x^3-1\right)+1\right]^{2/3}+\left[\frac{C^3}{A^3}\left(x^3-1\right)+1\right]^{1/3}} \\ &- \frac{\mu^{(2)}}{\rho C^2}\left(x^3-1\right)\frac{2\frac{x^3+\gamma}{1+\gamma}-1}{\frac{x^3+\gamma}{1+\gamma}+\left(\frac{x^3+\gamma}{1+\gamma}\right)^{2/3}+\left(\frac{x^3+\gamma}{1+\gamma}\right)^{1/3}}. \end{aligned} \tag{98}$$

The above function is monotonically decreasing for $0<x<1$ and increasing for $x>1$. When $\mu^{(1)}=\mu^{(2)}$, the function corresponding to a homogeneous spherical shell is obtained [42].

Assuming that $\mu^{(1)}$ and $\mu^{(2)}$ have a constant lower bound $\eta>0$, it follows that

$$\lim_{x\to 0} H(x,\gamma) = \lim_{x\to\infty} H(x,\gamma) = \infty. \tag{99}$$

We consider the following two cases:

(i) If $p_0=0$ and $C_0>0$, then equation (91) has exactly two solutions, $x=x_1$ and $x=x_2$, satisfying $0<x_1<1<x_2<\infty$, for any positive constant C_0. An example is shown in Figure 10, where $C_0=7$. These oscillations are not 'free' in general, since, by (78), if $T_{rr}(r,t)=0$ at $r=c$ and $r=b$, so that $T_1(t)=T_2(t)=0$, then $T_{\theta\theta}(r,t)=T_{\phi\phi}(r,t)\neq 0$ at $r=c$ and $r=b$, unless $r^2/R^2\to 1$.

(ii) When $p_0\neq 0$ and $C_0\geq 0$, substitution of (98) in (91) implies that the necessary and sufficient condition for the motion to be oscillatory is that p_0 satisfies

$$-\infty = \lim_{x\to 0}\frac{3\left(H(x,\gamma)-C_0\right)}{x^3-1} < p_0 < \sup_{0<x<\infty}\frac{3\left(H(x,\gamma)-C_0\right)}{x^3-1}, \tag{100}$$

where "sup" denotes supremum. This case is exemplified in Figure 11 where $p_0=1$ and $C_0=1$.

Thin-walled shell. In particular, when the shell wall is thin, such that $0<\gamma\ll 1$, if we assume that $A^3/C^3=B^3/A^3=\gamma/2+1$, then the problem reduces to that of a thin-walled homogeneous spherical shell with shear modulus $\left(\mu^{(1)}+\mu^{(2)}\right)/2$ [42].

4.2.2 Composite with two concentric homogeneous spherical shells subject to dead-load traction

We further assume that the outer circular surface of the composite tube is free, such that $T_2(t)=0$, while the inner surface is subject to a dead-load pressure $P_1(t)$ satisfying

$$2\frac{P_1(t)}{\rho C^2} = 2x^2\frac{T_1(t)}{\rho C^2} = \begin{cases} 0 & \text{if } t\leq 0, \\ p_0 & \text{if } t>0, \end{cases} \tag{101}$$

with p_0 constant in time. Integrating (85) implies

$$\dot{x}^2x^3\left[1-\left(1+\frac{\gamma}{x_0^3}\right)^{-1/3}\right] + H(x,\gamma) = p_0\left(x-1\right)+C_0, \tag{102}$$

where $H(x,\gamma)$ is given by (86), and

$$C_0 = \dot{x}_0^2x_0^3\left[1-\left(1+\frac{\gamma}{x_0^3}\right)^{-1/3}\right] + H(x_0,\gamma) - p_0\left(x_0-1\right), \tag{103}$$

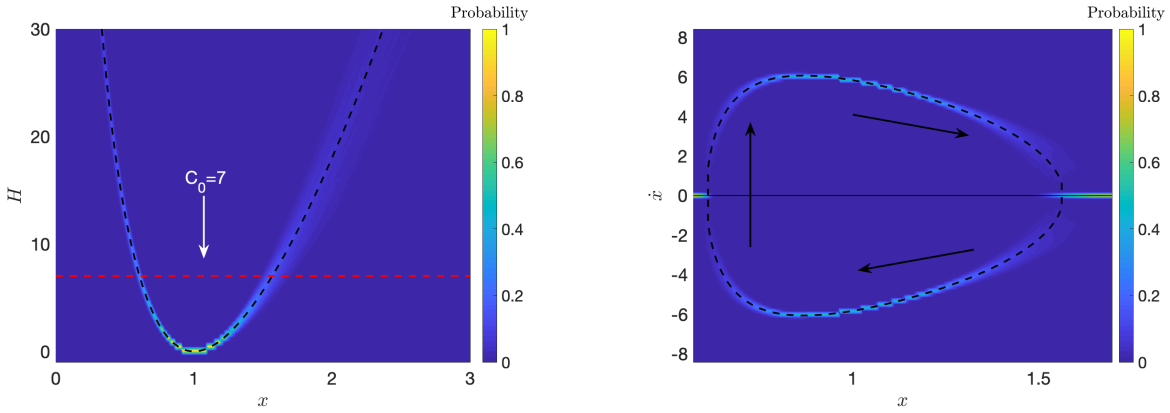

Figure 10: The function $H(x,\gamma)$, defined by (98), intersecting the (dashed red) line $C_0 = 7$ (left), and the associated velocity, given by (90) (right), for a dynamic composite tube with two concentric stochastic neo-Hookean phases, with inner radii $A = 1$ and $C = 1/2$, respectively, assuming that $\rho = 1$ and $\mu^{(1)}$ follows a Gamma distribution with $\rho_1^{(1)} = 405$ and $\rho_2^{(1)} = 4.05/\rho_1^{(1)} = 0.01$, while $\mu^{(2)}$ is drawn from a Gamma distribution with $\rho_1^{(2)} = 405$ and $\rho_2^{(2)} = 4.2/\rho_1^{(2)}$. The dashed black lines correspond to the expected values based only on mean values, $\underline{\mu}^{(1)} = 4.05$ and $\underline{\mu}^{(2)} = 4.2$. Each distribution was calculated from the average of 1000 stochastic simulations.

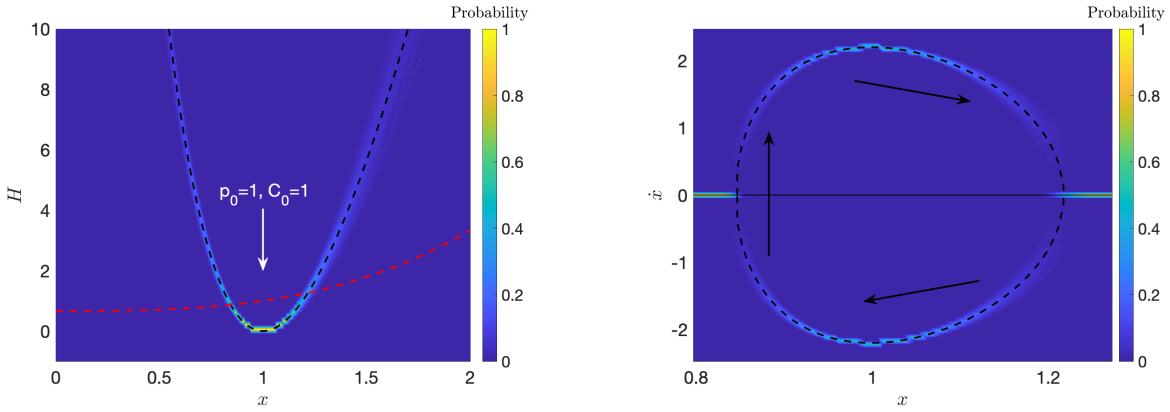

Figure 11: The function $H(x,\gamma)$, defined by (98), intersecting the (dashed red) line $\frac{p_0}{3}\left(x^3-1\right)+C_0$ when $p_0 = 1$ and $C_0 = 1$ (left), and the associated velocity, given by (90) (right), for a dynamic composite tube with two concentric stochastic neo-Hookean phases, with inner radii $A = 1$ and $C = 1/2$, respectively, under impulse traction, assuming that $\rho = 1$ and $\mu^{(1)}$ follows a Gamma distribution with $\rho_1^{(1)} = 405$ and $\rho_2^{(1)} = 4.05/\rho_1^{(1)} = 0.01$, while $\mu^{(2)}$ is drawn from a Gamma distribution with $\rho_1^{(2)} = 405$ and $\rho_2^{(2)} = 4.2/\rho_1^{(2)}$. The dashed black lines correspond to the expected values based only on mean values, $\underline{\mu}^{(1)} = 4.05$ and $\underline{\mu}^{(2)} = 4.2$. Each distribution was calculated from the average of 1000 stochastic simulations.

with the initial conditions $x(0) = x_0$ and $\dot{x}(0) = \dot{x}_0$. From (88), we obtain the velocity

$$\dot{x} = \pm \sqrt{\frac{p_0\,(x-1) + C_0 - H(x,\gamma)}{x^3\left[1 - \left(1 + \frac{\gamma}{x^3}\right)^{-1/3}\right]}}. \tag{104}$$

Oscillatory motion of the composite spherical shell is observed if and only if the equation

$$H(x,\gamma) = p_0\,(x-1) + C_0, \tag{105}$$

has exactly two distinct solutions, representing the amplitudes of the oscillation, $x = x_1$ and $x = x_2$, such that $0 < x_1 < x_2 < \infty$. In this case, the minimum and maximum radii of the inner surface in the oscillation are given by $x_1 A$ and $x_2 A$, respectively, and the period of oscillation is equal to

$$T = 2\left|\int_{x_1}^{x_2} \frac{\mathrm{d}x}{\dot{x}}\right| = 2\left|\int_{x_1}^{x_2} \sqrt{\frac{x^3\left[1 - \left(1 + \frac{\gamma}{x^3}\right)^{-1/3}\right]}{p_0\,(x-1) + C_0 - H(x,\gamma)}}\mathrm{d}x\right|. \tag{106}$$

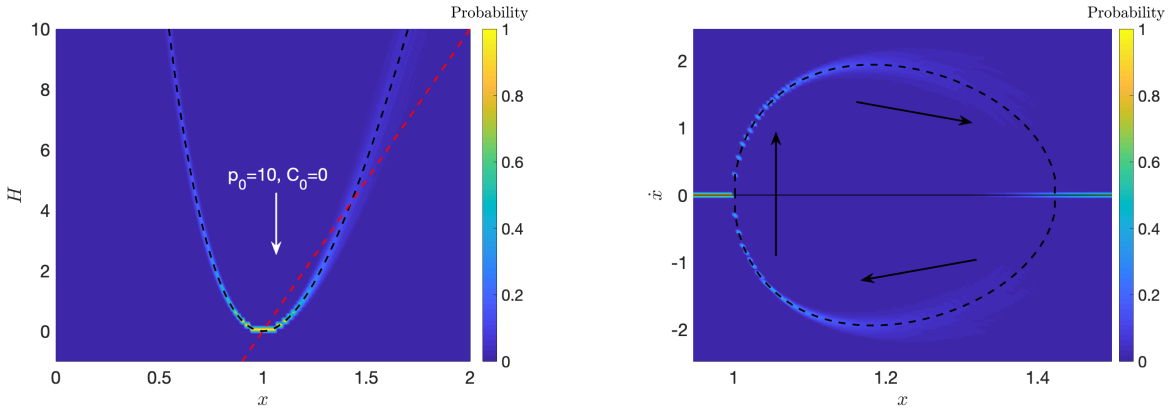

Figure 12: The function $H(x,\gamma)$, defined by (98), intersecting the (dashed red) line $p_0\,(x-1)+C_0$ when $p_0 = 10$ and $C_0 = 0$ (left), and the associated velocity, given by (90) (right), for a dynamic composite tube with two concentric stochastic neo-Hookean phases, with inner radii $A = 1$ and $C = 1/2$, respectively, under dead-load traction, assuming that $\rho = 1$ and $\mu^{(1)}$ follows a Gamma distribution with $\rho_1^{(1)} = 405$ and $\rho_2^{(1)} = 4.05/\rho_1^{(1)} = 0.01$, while $\mu^{(2)}$ is drawn from a Gamma distribution with $\rho_1^{(2)} = 405$ and $\rho_2^{(2)} = 4.2/\rho_1^{(2)}$. The dashed black lines correspond to the expected values based only on mean values, $\underline{\mu}^{(1)} = 4.05$ and $\underline{\mu}^{(2)} = 4.2$. Each distribution was calculated from the average of 1000 stochastic simulations.

The case with $p_0 = 0$ is similar to that when an impulse traction was assume. For $p_0 \neq 0$ and $C_0 \geq 0$, substitution of (98) in (91) implies that the necessary and sufficient condition for the motion to be oscillatory is that p_0 satisfies

$$-\infty = \lim_{x\to 0} \frac{(H(x,\gamma) - C_0)}{x-1} < p_0 < \sup_{0<x<\infty} \frac{(H(x,\gamma) - C_0)}{x-1} = +\infty. \tag{107}$$

An example is shown in Figure 12, where $p_0 = 5$ and $C_0 = 0$, and the geometric and material parameters for the composite tube are as in the previous case.

4.3 Oscillatory motion of a stochastic radially-inhomogeneous spherical shell

We also examine the oscillatory motion of radially inhomogeneous incompressible spherical shells of stochastic hyperelastic material described by a neo-Hookean-like strain-energy function, with the constitutive parameter varying continuously along the radial direction. Similarly to the case of a

radially inhomogeneous tube, the radially inhomogeneous sphere can be regarded as an extension of the composite with two concentric phases to the case with infinitely many concentric layers and continuous inhomogeneity. Our inhomogeneous model is similar to those proposed in [49], where the cavitation and radial oscillatory motion of a stochastic sphere was treated explicitly.

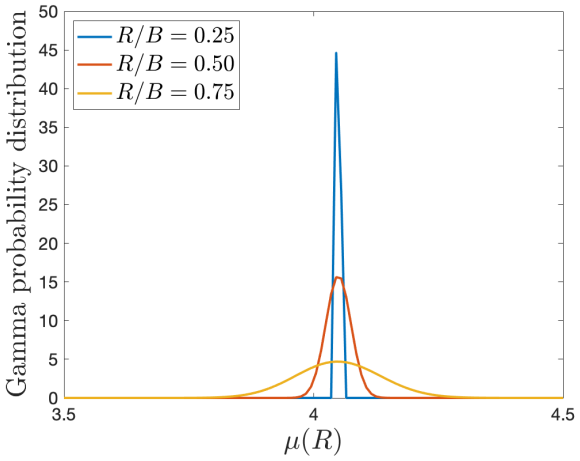

Figure 13: Examples of Gamma distribution, with hyperparameters $\rho_1 = 405 \cdot B^6/R^6$ and $\rho_2 = 0.01 \cdot R^6/B^6$, for the shear modulus $\mu(R)$ given by (108).

Here, we define the class of stochastic inhomogeneous hyperelastic models (1) with the shear modulus taking the form (see also [17])

$$\mu(R) = C_1 + C_2 \frac{R^3}{C^3}, \tag{108}$$

where $\mu(R) > 0$, for all $C \le R \le B$, $C_1 > 0$ is a single-valued (deterministic) constant, and C_2 is a random value defined by a given probability distribution.

When the mean value of the shear modulus $\mu(R)$, described by (108), does not depend on R, as C_1, R and C are deterministic and C_2 is probabilistic, we have

$$\underline{\mu} = C_1, \qquad \mathrm{Var}[\mu] = \mathrm{Var}[C_2] \frac{R^6}{C^6}, \tag{109}$$

where $\mathrm{Var}[C_2]$ is the variance of C_2, while the mean value of C_2 is $\underline{C}_2 = 0$.

By (3) and (109), the hyperparameters of the corresponding Gamma distribution, defined by (4), take the form

$$\rho_1 = \frac{C_1}{\rho_2}, \qquad \rho_2 = \frac{\mathrm{Var}[\mu]}{C_1} = \frac{\mathrm{Var}[C_2]}{C_1} \frac{R^6}{C^6}. \tag{110}$$

For example, we can choose two constant values, $C_0 > 0$ and $C_1 > 0$, and set the hyperparameters for the Gamma distribution at any given R as follows,

$$\rho_1 = \frac{C_1}{C_0} \frac{C^6}{R^6}, \qquad \rho_2 = C_0 \frac{R^6}{C^6}. \tag{111}$$

By (108), $C_2 = (\mu(R) - C_1)\, C^3/R^3$ is the shifted Gamma-distributed random variable with mean value $\underline{C}_2 = 0$ and variance $\mathrm{Var}[C_2] = \rho_1 \rho_2^2 C^6/R^6 = C_0 C_1$.

In Figure 13, we show Gamma distributions with $\rho_1 = 405 \cdot B^6/R^6$ and $\rho_2 = 0.01 \cdot R^6/B^6$. By (108) and (111), $C_0 = 0.01 \cdot C^6/B^6$, $C_1 = \underline{\mu} = \rho_1 \rho_2 = 4.05$ and $C_2 = \mu(C) - C_1$. In particular, for a shell with infinitely thick wall, as R decreases to C, ρ_1 increases, while ρ_2 decreases, and the Gamma distribution converges to a normal distribution [18, 41].

The shear modulus defined by (108) can be expressed equivalently as

$$\mu(u) = C_1 + C_2 \frac{x^3 - 1}{u - 1}, \tag{112}$$

where $u = r^3/R^3$ and $x = c/C$, as denoted in (81).

Next, writing the invariants given by (73) in the equivalent form

$$I_1 = u^{-4/3} + 2u^{2/3}, \qquad I_2 = u^{4/3} + 2u^{-2/3}, \qquad I_3 = 1, \tag{113}$$

and substituting these in (75) gives

$$\begin{aligned} \beta_1 &= 2\frac{\partial W}{\partial I_1} = \mu + \frac{d\mu}{\mathrm{d}u}\frac{\mathrm{d}u}{\mathrm{d}I_1}\left(I_1 - 3\right), \\ \beta_{-1} &= -2\frac{\partial W}{\partial I_2} = -\frac{\mathrm{d}\mu}{\mathrm{d}u}\frac{\mathrm{d}u}{\mathrm{d}I_2}\left(I_1 - 3\right), \end{aligned} \tag{114}$$

where μ is defined by (112). Therefore,

$$\begin{aligned} \beta_1 &= C_1 + \frac{3C_2}{4}\frac{x^3-1}{u-1}\left[\frac{4}{3} - \frac{2u^3 - 3u^{7/3} + u}{(u-1)^2(u+1)}\right], \\ \beta_{-1} &= \frac{3C_2}{4}\frac{x^3-1}{u-1}\frac{2u^{7/3} - 3u^{5/3} + u^{1/3}}{(u-1)^2(u+1)}, \end{aligned} \tag{115}$$

and

$$\beta_1 - \beta_{-1}\frac{r^2}{R^2} = C_1 + \frac{3C_2}{2}\frac{x^3-1}{u-1}\left[\frac{2}{3} - \frac{2u^3 - 3u^{7/3} + u}{(u-1)^2(u+1)}\right]. \tag{116}$$

Recalling the stress components described by (78), and following a similar approach as in the previous section, we set the pressure impulse as in (87). Then, similarly to (86), using (116), we define the function

$$\begin{aligned} H(x,\gamma) &= \frac{4C_1}{3\rho C^2}\int_1^x \left(\zeta^2 \int_{\frac{\zeta^3+\gamma}{1+\gamma}}^{\zeta^3} \frac{1+u}{u^{7/3}}\mathrm{d}u\right)\mathrm{d}\zeta \\ &\quad + \frac{2C_2}{\rho C^2}\int_1^x \left\{\left(\zeta^5 - \zeta^2\right)\int_{\frac{\zeta^3+\gamma}{1+\gamma}}^{\zeta^3} \frac{1+u}{u^{7/3}(u-1)}\left[\frac{2}{3} - \frac{2u^3 - 3u^{7/3} + u}{(u-1)^2(u+1)}\right]\mathrm{d}u\right\}\mathrm{d}\zeta \\ &= \frac{C_1}{\rho C^2}\left(x^3-1\right)\left[\frac{2x^3-1}{x^3+x^2+x} - \frac{2\frac{x^3+\gamma}{1+\gamma} - 1}{\frac{x^3+\gamma}{1+\gamma} + \left(\frac{x^3+\gamma}{1+\gamma}\right)^{2/3} + \left(\frac{x^3+\gamma}{1+\gamma}\right)^{1/3}}\right] \\ &\quad + \frac{C_2}{\rho C^2}\int_1^x \left(\zeta^5 - \zeta^2\right)\left[\frac{2\zeta^6 - 3\zeta^4 + 1}{\zeta^4\left(\zeta^3-1\right)^2} - \frac{2\left(\frac{\zeta^3+\gamma}{1+\gamma}\right)^2 - 3\left(\frac{\zeta^3+\gamma}{1+\gamma}\right)^{4/3} + 1}{\left(\frac{\zeta^3+\gamma}{1+\gamma}\right)^{4/3}\left(\frac{\zeta^3+\gamma}{1+\gamma} - 1\right)^2}\right]\mathrm{d}\zeta. \end{aligned} \tag{117}$$

We focus our attention on the following limiting cases:

Thick-walled shell. If the shell has an infinitely thick wall, such that $\gamma \to \infty$, then (117) takes the form

$$\begin{aligned} H(x) &= \frac{C_1}{\rho C^2}\left(x^3-1\right)\left(\frac{2x^3-1}{x^3+x^2+x} - \frac{1}{3}\right) \\ &\quad + \frac{C_2}{\rho C^2}\int_1^x \frac{2\zeta^6 - 3\zeta^4 + 1}{\zeta^2\left(\zeta^3-1\right)}\mathrm{d}\zeta \\ &= \frac{C_1}{\rho C^2}\left(x^3-1\right)\left(\frac{2x^3-1}{x^3+x^2+x} - \frac{1}{3}\right) \\ &\quad + \frac{C_2}{\rho C^2}\left[x^2 + \frac{1}{x} - \frac{3}{2}\log\left(x^2+x+1\right) + \sqrt{3}\arctan\frac{2x+1}{\sqrt{3}} - 2 + 3\log\sqrt{3} - \frac{\pi}{\sqrt{3}}\right]. \end{aligned} \tag{118}$$

Examples are presented in Figure 14 for the case without impulse or dead-load traction, in Figure 15 for the case when the pressure impulse is given by (87), and in Figure 16 for the case when the dead-load traction is given by (101).

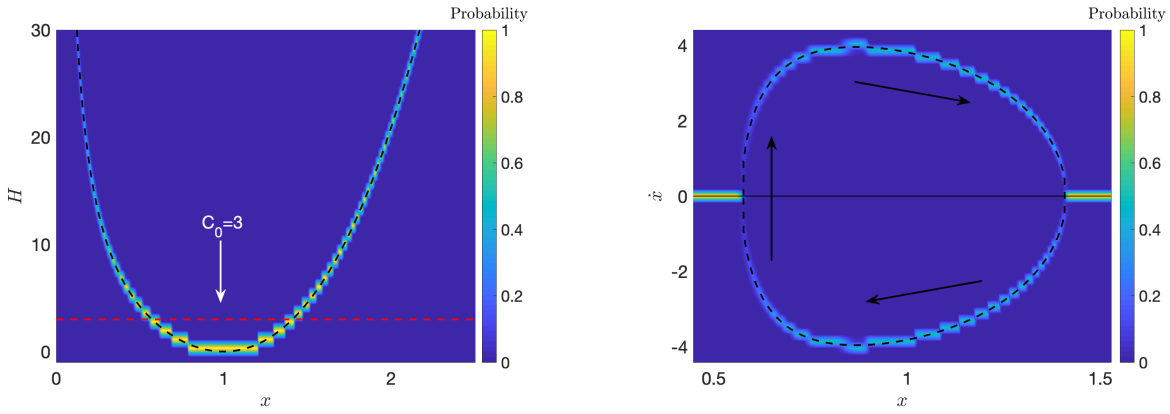

Figure 14: The function $H(x, \gamma)$, defined by (118), intersecting the (dashed red) line $C_0 = 3$ (left), and the associated velocity, given by (90) (right), for a dynamic radially inhomogeneous shell with infinitely thick wall having inner radius $C = 1$, assuming that $\rho = 1$ and μ follows a Gamma distribution with $\rho_1 = 405/R^6$ and $\rho_2 = 0.01 \cdot R^6$. The dashed black lines correspond to the expected values based only on mean values. Each distribution was calculated from the average of 1000 stochastic simulations.

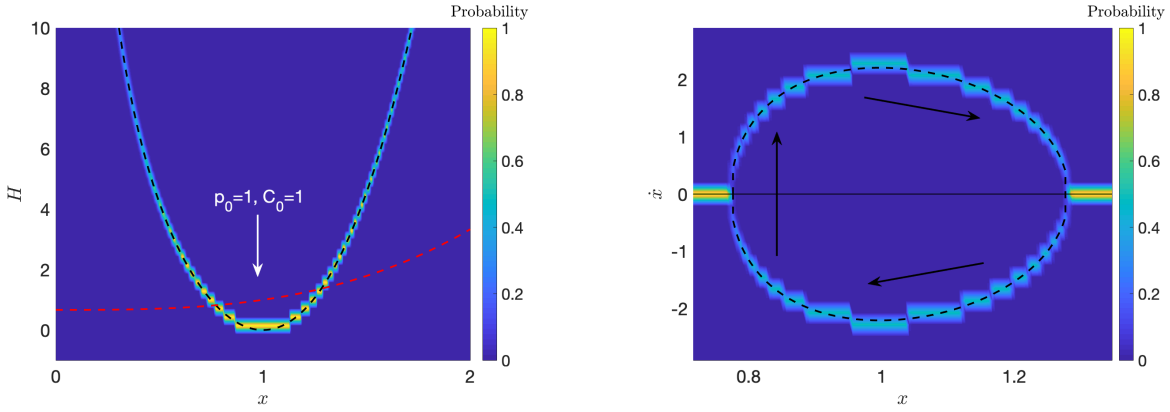

Figure 15: The function $H(x, \gamma)$, defined by (118), intersecting the (dashed red) line $\frac{p_0}{3}\left(x^3 - 1\right) + C_0$ when $p_0 = 1$ and $C_0 = 1$ (left), and the associated velocity, given by (90) (right), for a dynamic radially inhomogeneous shell with infinitely thick wall having inner radius $C = 1$, under impulse traction, assuming that $\rho = 1$ and μ follows a Gamma distribution with $\rho_1 = 405/R^6$ and $\rho_2 = 0.01 \cdot R^6$. The dashed black lines correspond to the expected values based only on mean values. Each distribution was calculated from the average of 1000 stochastic simulations.

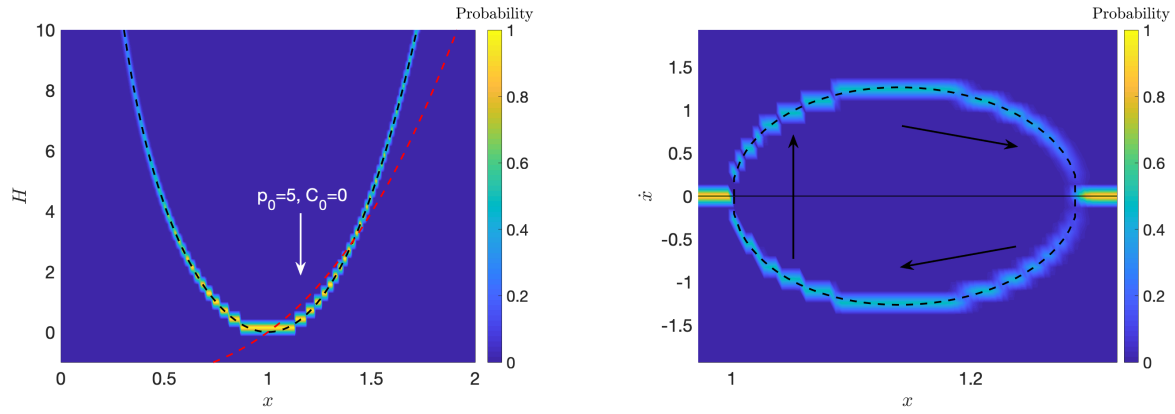

Figure 16: The function $H(x,\gamma)$, defined by (118), intersecting the (dashed red) line $p_0\,(x-1)+C_0$ when $p_0=5$ and $C_0=0$ (left), and the associated velocity, given by (90) (right), for a dynamic radially inhomogeneous shell with infinitely thick wall having inner radius $C=1$, under dead-load traction, assuming that $\rho=1$ and μ follows a Gamma distribution with $\rho_1=405/R^6$ and $\rho_2=0.01\cdot R^6$. The dashed black lines correspond to the expected values based only on mean values. Each distribution was calculated from the average of 1000 stochastic simulations.

Thin-walled shell. If the shell wall is thin, such that $0<\gamma\ll 1$, then the shear modulus defined by (108) takes the form $\mu=C_1+C_2$, and the problem reduces to that of a homogeneous shell with thin wall (see also [42]).

5 Conclusion

We have studied analytically the dynamic inflation and finite amplitude oscillatory motion of composite cylindrical tubes and spherical shells with two concentric stochastic homogeneous neo-Hookean phases, and of inhomogeneous tubes and shells of neo-Hookean-like material with the constitutive parameter varying continuously in the radial direction. For the homogeneous materials, the shear moduli are (spatially-independent) random variables, while for the radially inhomogeneous bodies, the shear moduli are (spatially-dependent) random fields, described by Gamma probability density functions. We obtain that, under radially-symmetric dynamic deformation, treated as quasi-equilibrated motion, these bodies oscillate (i.e., their radius increases up to a point, then decreases, then increases again, and so on), and the amplitude and period of the oscillations are characterised by probability distributions, depending on the initial conditions, the geometry, and the probabilistic material properties. These results extend previous theoretical findings for cylindrical tubes and spherical shells of stochastic hyperelastic material with spatially-independent elastic parameters [41, 42].

The particular values of the stochastic parameters in our numerical calculations are for illustrative purposes only. The propagation of stochastic variation from input material parameters to output mechanical behaviour is mathematically traceable, offering valuable insights into how probabilistic approaches can be incorporated into the nonlinear elasticity theory. Other stochastic hyperelastic models, such as those defined in [46], can also be used instead of the neo-Hookean model. However, for compressible materials, the theorem on quasi-equilibrated dynamics is not applicable [75, p. 209]. As our analytical approach relies on the notion of quasi-equilibrated motion for incompressible cylindrical tubes and spherical shells, the same approach cannot be used for the compressible case. Nevertheless, standard elastodynamic problems can be formulated, and then treated numerically. Extensions to more realistic models of stochastic heterogeneous bodies also require computational tools. Our stochastic analysis can further be extended to other inflation instabilities, such as localised bulging in inflated circular cylindrical tubes [19, 78]. This is likely to occur for all isotropic material models when the axial stretch is fixed and below a certain threshold value depending on the constitutive model.

Declaration of Competing Interest. The authors declare that they have no known competing financial interests or personal relationships that could have appeared to influence the work reported in this paper.

Credit Authorship Contribution Statement. L. Angela Mihai: conceptualization, investigation, methodology, supervision, writing - original draft & review. Manal Alamoudi: formal analysis, investigation, writing - original draft & review.

Acknowledgement. We gratefully acknowledge the scholarship from the Saudi Arabia Government to Manal Alamoud, and the support by the Engineering and Physical Sciences Research Council of Great Britain under research grant EP/S028870/1 to L. Angela Mihai.

References

[1] Abramowitz M, Stegun IA. 1964. Handbook of Mathematical Functions with Formulas, Graphs, and Mathematical Tables, National Bureau of Standards, Applied Mathematics Series, vol. 55, U.S. Government Printing Office, Washington, D.C.

[2] Adkins JE, Rivlin RS. 1952. Large elastic deformations of isotropic materials. IX. The deformation of thin shells, Philosophical Transactions of the Royal Society of London A 244, 505-531.

[3] Alijani F, Amabili M. 2014. Non-linear vibrations of shells: A literature review from 2003 to 2013, International Journal of Non-Linear Mechanics 58, 233-257.

[4] Amabili M. 2008. Nonlinear Vibrations and Stability of Shells and Plates, Cambridge University Press, Cambridge.

[5] Baker M, Ericksen JL. 1954. Inequalities restricting the form of stress-deformation relations for isotropic elastic solids and Reiner-Rivlin fluids, Journal of the Washington Academy of Sciences 44(2), 33-35.

[6] Balakrishnan R, Shahinpoor M. 1978. Finite amplitude oscillations of a hyperelastic spherical cavity, International Journal of Non-Linear Mechanics 13, 171-176.

[7] Bayes T. 1763. An essay toward solving a problem in the doctrine of chances, Philosophical Transactions of the Royal Society 53, 370-418.

[8] Beatty MF. 2007. On the radial oscillations of incompressible, isotropic, elastic and limited elastic thick-walled tubes, International Journal of Non-Linear Mechanics 42, 283-297.

[9] Beatty MF. 2011. Small amplitude radial oscillations of an incompressible, isotropic elastic spherical shell, Mathematics and Mechanics of Solids 16, 492-512.

[10] Breslavsky I, Amabili M. 2018. Nonlinear vibrations of a circular cylindrical shell with multiple internal resonances under multi-harmonic excitation, Nonlinear Dynamics 93, 53-62.

[11] Brewick PT, Teferra K. 2018. Uncertainty quantification for constitutive model calibration of brain tissue, Journal of the Mechanical Behavior of Biomedical Materials 85, 237-255.

[12] Carroll MM. 1987. Pressure maximum behavior in inflation of incompressible elastic hollow spheres and cylinders. Quarterly of Applied Mathematics 45, 141-154.

[13] Caylak I, Penner E, Dridger A, Mahnken R. 2018. Stochastic hyperelastic modeling considering dependency of material parameters, Computational Mechanics 62, 1273-1285 (doi: 10.1007/s00466-018-1563-z).

[14] Dong YH, Zhu B, Wang Y, Li YH, Yang J. 2018. Nonlinear free vibration of graded graphene reinforced cylindrical shells: Effects of spinning motion and axial load, Journal of Sound and Vibration 437, 79-96.

[15] Elishakoff I. 2017. Probabilistic Methods In The Theory Of Structures: Strength Of Materials, Random Vibrations, And Random Buckling, 3rd ed, World Scientific Publishing Co., Singapore.

[16] Elishakoff I. 2017. Problems Book for Probabilistic Methods for the Theory of Structures with Complete Worked Through Solutions, World Scientific Publishing Co., Singapore.

[17] Ertepinar A, Akay HU. 1976. Radial oscillations of nonhomogeneous, thick-walled cylindrical and spherical shells subjected to finite deformations, International Journal of Solids and Structures 12, 517-524.

[18] Fitt D, Wyatt H, Woolley TE, Mihai LA. 2019. Uncertainty quantification of elastic material responses: testing, stochastic calibration and Bayesian model selection, Mechanics of Soft Materials 1, 1-13 (doi: 10.1007/s42558-019-0013-1).

[19] Fu YB, Liu JL, Francisco GS. 2016. Localized bulging in an inflated cylindrical tube of arbitrary thickness - the effect of bending stiffness, Journal of the Mechanics and Physics of Solids 90, 45-60.

[20] Ghanem R, Higdon D, Owhadi H (Eds.). 2017. Handbook of Uncertainty Quantification. Springer, New-York, 2017.

[21] Goriely A. 2017. The Mathematics and Mechanics of Biological Growth, Springer-Verlag, New York.

[22] Goriely A, Destrade M, Ben Amar M. 2006. Instabilities in elastomers and in soft tissues, The Quarterly Journal of Mechanics and Applied Mathematics 59, 615-630.

[23] Green AE, Shield RT. 1950. Finite elastic deformations in incompressible isotropic bodies, Proceeding of the Royal Society of London A 202, 407-419.

[24] Grimmett GR, Stirzaker DR. 2001. Probability and Random Processes, 3rd ed, Oxford University Press, Oxford.

[25] Guilleminot J. 2020. Modelling non-Gaussian random fields of material properties in multiscale mechanics of materials, in Uncertainty Quantification in Multiscale Materials Modeling, Y. Wang and F.L. McDowell (Eds.), Elsevier, Cambridge, MA.

[26] Heng GZ, Solecki R. 1963. Free and forced finite amplitude oscillations of an elastic thick-walled hollow sphere made of incompressible material, Archiwum Mechaniki Stosowanej 3, 427-433.

[27] Horgan CO, Pence TJ. 1989. Cavity formation at the center of a composite incompressible nonlinearly elastic sphere, Journal of Applied Mechanics 56, 302-308.

[28] Hughes I, Hase TPA. 2010. Measurements and Their Uncertainties: A Practical Guide to Modern Error Analysis, Oxford University Press, Oxford.

[29] Jaynes ET. 1957. Information theory and statistical mechanics i, Physical Review 108, 171-190.

[30] Jaynes ET. 1957. Information theory and statistical mechanics ii, Physical Review 106, 620-630.

[31] Jaynes ET. 2003. Probability Theory: The Logic of Science, Cambridge University Press, Cambridge, UK.

[32] Johnson NL, Kotz S, Balakrishnan N. 1994. Continuous Univariate Distributions, Vol 1, 2nd edition, John Wiley & Sons, New York.

[33] Kaminski M, Lauke B. 2018. Probabilistic and stochastic aspects of rubber hyperelasticity, Meccanica 53, 2363-2378.

[34] Knowles JK. 1960. Large amplitude oscillations of a tube of incompressible elastic material, Quarterly of Applied Mathematics 18, 71-77.

[35] Knowles JK. 1962. On a class of oscillations in the finite-deformation theory of elasticity, Journal of Applied Mechanics 29, 283-286.

[36] Knowles JK, Jakub MT. 1965. Finite dynamic deformations of an incompressible elastic medium containing a spherical cavity, Archive of Rational Mechanics and Analysis 18, 376-387.

[37] Marzano M. 1983. An interpretation of Baker-Ericksen inequalities in uniaxial deformation and stress, Meccanica 18, 233-235.

[38] Mathai AM. 1982. Storage capacity of a dam with Gamma type inputs, Annals of the Institute of Statistical Mathematics 34, 591-597.

[39] McCoy JJ. 1973. A statistical theory for predicting response of materials that possess a disordered structure, Technical report ARPA 2181, AMCMS Code 5911.21.66022, Army Materials and Mechanics Research Center, Watertown, Massachusetts.

[40] McGrayne SB. 2012. The Theory That Would Not Die: How Bayes' Rule Cracked the Enigma Code, Hunted Down Russian Submarines, an Emerged Triumphant from Two Centuries of Controversy, Paperback ed., Yale University Press, New Haven.

[41] Mihai LA, Fitt D, Woolley TE, Goriely A. 2019. Likely equilibria of stochastic hyperelastic spherical shells and tubes, Mathematics and Mechanics of Solids, 24(7), 2066-2082 (doi: 10.1177/1081286518811881).

[42] Mihai LA, Fitt D, Woolley TE, Goriely A. 2019. Likely oscillatory motions of stochastic hyperelastic solids, Transactions of Mathematics and Its Applications 3, 1-42 (doi: 10.1093/imatrm/tnz003).

[43] Mihai LA, Fitt D, Woolley TE, Goriely A. 2019. Likely cavitation in stochastic elasticity, Journal of Elasticity 137(1), 27-42 (doi: 10.1007/s10659-018-9706-1).

[44] Mihai LA, Goriely A. 2017. How to characterize a nonlinear elastic material? A review on nonlinear constitutive parameters in isotropic finite elasticity, Proceedings of the Royal Society A 473, 20170607 (doi: 10.1098/rspa.2017.0607).

[45] Mihai LA, Goriely A. 2020. Likely striping in stochastic nematic elastomers, Mathematics and Mechanics of Solids 25(10), 1851-1872 (doi: 0.1177/1081286520914958).

[46] Mihai LA, Woolley TE, Goriely A. 2018. Stochastic isotropic hyperelastic materials: constitutive calibration and model selection, Proceedings of the Royal Society A 474, 20170858.

[47] Mihai LA, Woolley TE, Goriely A. 2019. Likely equilibria of the stochastic Rivlin cube, Philosophical Transactions of the Royal Society A 377, 20180068 (doi: 10.1098/rsta.2018.0068).

[48] Mihai LA, Woolley TE, Goriely A. 2019. Likely chirality of stochastic anisotropic hyperelastic tubes, International Journal of Non-Linear Mechanics 114, 9-20 (doi: 10.1016/j.ijnonlinmec.2019.04.004).

[49] Mihai LA, Woolley TE, Goriely A. 2020. Likely cavitation and radial motion of stochastic elastic spheres, Nonlinearity 33(5), 1987-2034.

[50] Moschopoulos PG. 1985. The distribution of the sum of independent Gamma random variables, Annals of the Institute of Statistical Mathematics 37(3), 541-544.

[51] Müller I, Struchtrup H. 2002. Inflation of rubber balloon, Mathematics and Mechanics of Solids 7, 569-577.

[52] Nörenberg N, Mahnken R. 2015. Parameter identification for rubber materials with artificial spatially distributed data, Computational Mechanics 56, 353370.

[53] Oden JT. 2018. Adaptive multiscale predictive modelling, Acta Numerica 27, 353-450.

[54] Ogden RW. 1997. Non-Linear Elastic Deformations, 2nd ed, Dover, New York.

[55] Ostoja-Starzewski M. 2007. Microstructural Randomness and Scaling in Mechanics of Materials, Taylor & Francis Group, Boca Raton, FL.

[56] Rivlin RS. 1949. Large elastic deformations of isotropic materials. VI. Further results in the theory of torsion, shear and flexure, Philosophical Transactions of the Royal Society of London A 242(845), 173-195.

[57] Robert CP. 2007. The Bayesian Choice: From Decision-Theoretic Foundations to Computational Implementation, 2nd ed, Springer, New York.

[58] Shahinpoor M. 1973. Combined radial-axial large amplitude oscillations of hyperelastic cylindrical tubes, Journal of Mathematical and Physical Sciences 7, 111-128.

[59] Shannon CE. 1948. A mathematical theory of communication, Bell System Technical Journal 27, 379-423, 623-659.

[60] Shield RT. 1972. On the stability of finitely deformed elastic membranes. II: Stability of inflated cylindrical and spherical membranes, Zeitschrift für Angewandte Mathematik und Physik (ZAMP) 23, 16-34.

[61] Sivaloganathan, I. 1991. Cavitation, the incompressible limit, and material inhomogeneity, Quarterly of Applied Mathematics 49, 521-541.

[62] Soize C. 2000. A nonparametric model of random uncertainties for reduced matrix models in structural dynamics, Probabilistic Engineering Mechanics 15, 277-294.

[63] Soize C. 2001. Maximum entropy approach for modeling random uncertainties in transient elastodynamics, Journal of the Acoustical Society of America 109, 1979-1996.

[64] Soize C. 2006. Non-Gaussian positive-definite matrix-valued random fields for elliptic stochastic partial differential operators, Computer Methods in Applied Mechanics and Engineering 195, 26-64.

[65] Soize C. 2013. Stochastic modeling of uncertainties in computational structural dynamics - Recent theoretical advances, Journal of Sound and Vibration 332, 2379-2395.

[66] Soize C. 2017. Uncertainty Quantification: An Accelerated Course with Advanced Applications in Computational Engineering, Interdisciplinary Applied Mathematics Book 47, Springer, New York.

[67] Soni J, Goodman R. 2017. A Mind at Play: How Claude Shannon Invented the Information Age, Simon & Schuster, New York.

[68] Staber B, Guilleminot J. 2015. Stochastic modeling of a class of stored energy functions for incompressible hyperelastic materials with uncertainties, Comptes Rendus Mécanique 343, 503-514.

[69] Staber B, Guilleminot J. 2016. Stochastic modeling of the Ogden class of stored energy functions for hyperelastic materials: the compressible case, Journal of Applied Mathematics and Mechanics/Zeitschrift für Angewandte Mathematik und Mechanik 97, 273-295.

[70] Staber B, Guilleminot J. 2017. Stochastic hyperelastic constitutive laws and identification procedure for soft biological tissues with intrinsic variability, Journal of the Mechanical Behavior of Biomedical Materials 65, 743-752.

[71] Staber B, Guilleminot J. 2018. A random field model for anisotropic strain energy functions and its application for uncertainty quantification in vascular mechanics, Computer Methods in Applied Mechanics and Engineering 333, 94-113.

[72] Staber B, Guilleminot J, Soize C, Michopoulos J, Iliopoulos A. 2019. Stochastic modeling and identification of an hyperelastic constitutive model for laminated composites, Computer Methods in Applied Mechanics and Engineering 347, 425-444.

[73] Sullivan TJ. 2015. Introduction to Uncertainty Quantification, Springer-Verlag, New York.

[74] Truesdell C. 1962. Solutio generalis et accurata problematum quamplurimorum de motu corporum elasticorum incomprimibilium in deformationibus valde magnis, Archive of Rational Mechanics and Analysis 11, 106-113.

[75] Truesdell C, Noll W. 2004. The Non-Linear Field Theories of Mechanics, 3rd ed, Springer-Verlag, New York.

[76] Vogel S. 1998. Cat's Paws and Catapults, WW Norton and Company, New York, London.

[77] Wang CC. 1965. On the radial oscillations of a spherical thin shell in the finite elasticity theory, Quarterly of Applied Mathematics 23, 270-274.

[78] Ye Y, Liu Y, Fu Y. 2020. Weakly nonlinear analysis of localized bulging of an inflated hyperelastic tube of arbitrary wall thickness, Journal of the Mechanics and Physics of Solids 135, 103804 (doi: 10.1016/j.jmps.2019.103804).

[79] Zamani V, Pence TJ. 2017. Swelling, inflation, and a swelling-burst instability in hyperelastic spherical shells, International Journal of Solids and Structures 125, 134-149.